A COMPARISON OF SOME ANALYTICAL MODELS WITH EXPERIMENT FOR THE UNIVERSITY OF MARYLAND REACTOR

by
Malcolm Fred Ross, Jr.

Thesis submitted to the Faculty of the Graduate School of the University of Maryland in partial fulfillment of the requirements for the degree of Master of Science
1968

APPROVAL SHEET

Title of Thesis: A Comparison of Some Analytical Models with Experiment for the University of Maryland Reactor

Name of Candidate: Malcolm Fred Ross, Jr.
Master of Science, 1968

Thesis and Abstract Approved: Dick Duffey

Dr. Dick Duffey
Professor of Nuclear Engineering

Date Approved:
9 Jan 1968

ABSTRACT

Title of Thesis: A Comparison of Some Analytical Models with Experiment for the University of Maryland Reactor

Malcolm Fred Ross, Jr., Master of Science

Thesis directed by: Dr. Dick Duffey

It is often desirable in the operation of a research reactor to make adjustments in the nuclear core configuration. These adjustments may occur for a variety of reasons, such as the rearrangement of fuel to perform a particular experiment. It is beneficial to the reactor operator and experimenter to have an adequate analytical model with which to predict the changes in nuclear characteristics which occur with core rearrangement.

Several analytical models have been investigated and compared with experimental results for the semi-permanent, or normal, core configuration for the University of Maryland Reactor. These models were selected because, while somewhat time consuming with respect to the use of computers, the computer time utilized is much less than needed by more complex methods. At the same time, the methods used tend to minimize the large inherent error associated with simple hand calculations.

The methods used consist of a two-dimensional few group diffusion theory coupled with several cross section models from which macroscopic cross sections were obtained.

The cross section models used for the above thermal energy groups were the volume integrated P-1 method and the Fourier transform B-1 method. Thermal energy group cross sections were obtained using the Wigner-Wilkins model and the Maxwell-Boltzmann model.

The volume integrated P-1 model and the Wigner-Wilkins model coupled with the two-dimensional group diffusion method were found to give the best agreement with experiment for the semi-permanent core configuration. This model was then tested over a range of experiments. The conclusion of this analysis was that the model was capable of predicting, with reasonable accuracy, the changes in core reactivity with core rearrangement.

ACKNOWLEDGEMENTS

I wish to express my appreciation and sincere thanks to: Dr. J. Fisher for his help in interpreting the experimental data; and to the University of Maryland Computer Center for the extensive use of the facilities. I wish to especially thank my advisor, Dr. D. Duffey, for his advice and guidance which were essential for the completion of this thesis.

TABLE OF CONTENTS

LIST OF FIGURES

LIST OF TABLES

CHAPTER I

INTRODUCTION

It is often desirable in the operation of a nuclear reactor, particularly a research reactor, to make adjustments in the nuclear core configuration. In a research reactor these adjustments may occur for a variety of reasons, such as the rearrangement of fuel to perform a particular experiment. Usually, the configuration chosen will be based on the desired nuclear characteristics as well as geometrical considerations. Typical examples of desirable nuclear characteristics for an experiment are maximizing the thermal neutron flux at a particular core location while retaining sufficient excess reactivity to allow a given power level.

It is beneficial to the reactor operator and the experimenter to have an adequate analytical model with which to predict the changes in nuclear characteristics which occur with core rearrangement. Though the final core analysis must rest with experiment, a mathematical model can be of use to the reactor operator as a guide to control rod movement, as well as for safety considerations, and can be a significant time saver to the experimenter in obtaining the desired nuclear characteristics.

The purpose of this research is to examine several analytical models with regard to application to the University of Maryland Reactor (UMR). The models investigated here neither require a prohibitive amount of computer

time nor are they dependent on simple hand calculations with sometimes large inherent error. The several models are examined on their ability to reproduce the neutron multiplication factor obtained experimentally for the University of Maryland Reactor. The most promising of the models is tested over a range of critical experiments with the reactor, which were performed prior to the analysis by Drs. D. Duffey,[1] J. Fisher and Mr. A. Diaz. Additional experiments performed by the author are also considered.

CHAPTER II

DESCRIPTION OF THE UNIVERSITY OF MARYLAND REACTOR

The University of Maryland Reactor is a heterogeneous light water moderated and cooled system and is operated at power levels up to 10 KW. The reactor core is located at the bottom of an open, water filled aluminum tank in the center of the shield structure.(2) The aluminum tank and shield are pierced by two beam tubes, a through tube, and a graphite thermal column. The tank provides for 17½ feet of water above the reactor core.

The reactor utilizes uranium fuel enriched to 93.5% uranium 235 (U-235) in the form of an uranium-aluminum alloy clad by aluminum in plate form. The reactor core is formed of 19 plate type fuel elements in a close packed array. A horizontal cross section of the reactor is shown in Fig. 1 in its semi-permanent or normal form. This semi-permanent core arrangement is composed of 14 regular assemblies containing 10 plates each, 4 partially loaded elements containing 6 plates each and 1 partially loaded element containing 5 plates. Each plate is 2.775 in. wide, .08 in. thick and 25.125 inches long. Non-fuel bearing plates are termed "dummy" plates. The fuel bearing, or meat, section of fuel plates is .026 in. thick, 2.469 in. wide and 23.625 in. long. The plates are located on a .263 in. pitch within a fuel element by means of spacers at the top and bottom. The plates associated with each element are in an aluminum can which is seated in a

bottom grid plate. Cross sectional views of a fully loaded assembly and the various partially loaded elements are shown in Fig. 3. The dimensions of the core elements are summarized in Table 1.

Two of the partially loaded fuel assemblies in the semi-permanent core configuration have four and five fuel plates removed to allow access into these core locations for experiments. These partially loaded assemblies are termed outer and inner irradiation spaces, or "glory holes", respectively. Each of the partial fuel assemblies contains an aluminum "dummy" plate which separates the experimental section of the assembly from the fuel bearing region to prevent fuel damage. The location of the inner and outer "glory holes" in the semi-permanent core arrangement is shown in Fig. 1.

There are 166 uranium bearing fuel plates in the semi-permanent core configuration. Of these plates, 147 contain 16 grams of U-235 per plate and 19 contain 18 grams of U-235 per plate. The 18 gram plates are located in the inner and outer "glory hole" elements and element F-8 as shown in Fig. 1. The total U-235 loading is 2671 grams. In addition to the "dummy" aluminum plates in the experimental assemblies there is a "dummy" plate in element C-4 located at the active core periphery (Fig. 1).

Reactor control is provided by two shim-safety rods and one regulating rod whose positions are shown in Fig. 1. The control rods operate within guide channels provided

by the absence of the four centrally located fuel plates in three of the partially loaded fuel assemblies. The shim-safety rods are used for gross control while the regulating rod provides fine adjustments. The regulating rod neutron absorbing, or poison, section is a stainless steel tube with pool water access through the top and bottom. The shim-safety rod poison sections are stainless steel tubes filled with boron carbide. The control rod positions are indicated to the nearest hundredth centimeter by three dials on the reactor console.

The core is reflected on top and bottom by water. In addition to the 19 fuel assemblies, there are 11 graphite elements in aluminum cans which provide a part of the side reflector. The reflector element dimensions are summarized in Table 1. The core and graphite assemblies form a 5 x 6 array (Fig. 1). The core and reflector elements are placed on a 3.189 in. pitch in the North-South plane, and a 3.035 in. pitch in the East-West direction. A cross section of a reflector element is shown in Fig. 3.

TABLE 1

CORE DIMENSIONS

Element Geometry

can spacing, in.	3.035 x 3.189
can wall thickness, in.	0.064
can inside dimension, in.	2.827

Table 1, Cont'd

Fuel Plate

plate width, in.	2.775
plate thickness, in.	0.080
plate height, in.	25.12
plate gap, in.	0.182
fuel bearing width, in.	2.469
fuel bearing thickness, in.	0.026
fuel bearing height, in.	23.62

Reflector Element

graphite can inside dimension, in.	2.669
graphite can wall thickness, in.	0.016
graphite can height, in.	25.25

CHAPTER III

THEORETICAL METHODS

The principal objective of this chapter is to describe the analytical models used in this study of the University of Maryland Reactor. The current methods used in analysis of critical experiments in the nuclear industry range from simple hand calculations to techniques that may require hours of digital computer time to obtain a solution.

A two-dimensional group diffusion technique is used in this analysis to calculate the neutron flux distribution and associated multiplication constant for the reactor. The major portion of the computational time required is due to the use of more than one dimension to describe the reactor, which is motivated by a strong desire to represent accurately the distribution of materials in the reactor. While this technique used is somewhat time consuming with computers, the time required is an order of magnitude less than for more complex methods. At the same time, the method is believed to minimize the large errors that may occur with hand calculations.

A. PDQ Model

1. Group Diffusion Equations. In the two-dimensional group diffusion method, the neutron energy spectrum is divided into a finite number of groups. The time independent differential equations of neutron diffusion are then assumed to hold for each of these groups. Solutions are

obtained for the time-independent group-diffusion equations using PDQ,[3] a two-dimensional reactor design code which finds a discrete numerical approximation for a heterogeneous reactor in either rectangular (X,Y) or cylindrical (R,Z) coordinates. The equations as typified in the PDQ code for the ith energy, or lethargy, group in rectangular coordinates are:[3]

$$-\nabla\cdot\left[D_1(\vec{r})\,\nabla\phi_i(\vec{r})\right]+\left[\Sigma_i^A(\vec{r})+\Sigma_i^R(\vec{r})+D_i(\vec{r})B_Z^2\right]\phi_i(\vec{r})=\frac{\chi_i\sum_{i=1}^{K}\nu\Sigma_i^f(\vec{r})\,\phi_i(\vec{r})+\Sigma_{i-1}^R(\vec{r})\,\phi_{i-1}(\vec{r})}{\lambda} \qquad (1)$$

where i, denoting the group number, goes from 1 to K with K denoting the thermal group. The total number of lethargy groups is to be less than or equal to four groups. The physical interpretation of the parameters in Eqn. 1 is:

D = the diffusion coefficient (cm)

Σ^A = the macroscopic absorption cross section (cm^{-1})

Σ^R = the macroscopic slowing down cross section (cm^{-1})

B_Z^2 = the group independent transverse buckling (cm^{-2})

χ_i = that fraction of fission neutrons appearing in the lethargy range represented by group i

ν = the average number of neutrons per fission

Σ^f = the macroscopic fission cross section (cm^{-1})

ϕ = the neutron flux (n/cm^2/sec)

λ = core multiplication constant

The physical representation of a heterogeneous reactor in the PDQ code is accomplished by dividing a two-dimensional rectangular region into subregions which represent the various material compositions present in the reactor. A constraint imposed by the code is that the physical parameters used in solving the neutron diffusion equations are assumed to be constant regionwise. Thus the group diffusion equations for a particular region in rectangular or X-Y coordinates become:

$$-D_i(\vec{r})\nabla^2\phi_i(\vec{r})+\left[\Sigma_i^A(\vec{r})+\Sigma_i^R(\vec{r})+D_i(\vec{r})B_Z^2\right]\phi_i(\vec{r}) = \frac{\chi_i\sum_{i=1}^{K}\nu\,\Sigma_i^f(\vec{r})\,\phi_i(\vec{r})+\Sigma_{i-1}^R(\vec{r})\,\phi_{i-1}(\vec{r})}{\lambda} \qquad (2)$$

The group diffusion equations in cylindrical (R,Z) coordinates are essentially the same as in rectangular (X,Y) coordinates, with the exception that the transverse leakage term in Eqns. 1 and 2 is zero. No angular dependence of neutron flux is considered.

The boundary conditions imposed at internal boundaries between regions are that the net current and flux are continuous across the interfaces. At external boundaries either the flux or net current may be set to zero depending upon the geometry and physical considerations of the problem.

Additional limitations placed upon the group diffusion equations given by 1 are that no neutron energy increase

from scattering, upscattering, can occur as well as that no scattering beyond a group range, through a group, is permitted. Therefore, the transfer of neutrons through energy can only proceed in a decreasing, or downward, direction between adjacent groups.

2. Core Representation for PDQ in Rectangular (X,Y) Geometry. The degree to which it is possible to represent the materials present in the core and reflector is guided, to some extent, by the storage capacity of the computer used for PDQ calculations. All calculations were performed on the IBM 7094 at the University of Maryland Computer Facility, which allows approximately 5300 spatial mesh points to represent the core and reflector components in the PDQ model. This representation is accomplished by the use of fifteen separate compositions or regions. Eight of these regions are used to represent core components while the remaining seven describe the reflector materials.

There are two distinct types of fuel regions described in the core, i.e. those associated with fuel loadings of 16 $\pm$0.2 and 18 $\pm$0.2 grams of U-235 per plate, respectively. These fuel regions are defined by a distance parallel to the plates equivalent to the length of the uranium-aluminum alloy meat, while the distance perpendicular to the plates is taken to be the number of fuel plates in the particular element times the distance from plate centerline to adjacent plate centerline. The fuel regions, as defined by this area, are a homogeneously volume averaged, or smeared, mixture of water, aluminum, U-235 and U-238.

The volume weighted nuclei, or number, densities are calculated for the fuel regions based on the materials present in the defining area. The loading uncertainty of ± 0.2 grams of U-235 per plate is neglected and the fuel loading per plate is calculated on the basis of the actual core loading of 2671 grams of U-235 for the semi-permanent core configuration. This corresponds to loadings of 15.86 grams and 17.85 grams of U-235 per plate, respectively, for these two kinds of plates.

The plate edges, i.e. the aluminum portion of the plate between the end of the uranium section and the edge of the plate, are homogenized with water. The volume weighted number densities for this region are calculated on the basis of an area defined in the direction parallel to the fuel plates by the distance between the edge of the fuel region and the inner face of the aluminum can. In the direction perpendicular to the fuel plates the defining distance is the same as the fuel region.

The "dummy" plate of aluminum in element C-4 is homogenized with water in the same proportion as a fuel plate. The "dummy" plates in the inner and outer "glory holes" are homogenized with somewhat different amounts of water to allow as accurately as possible a representation of the water in these elements. The aluminum cans which house the fuel elements are represented explicitly. The remaining core water not already present in the different homogenized regions is also represented explicitly. This water consists of that present between the aluminum cans, in the control rod channels, "glory holes", and that which is present between the outer

edge of the fuel region in the direction perpendicular to the fuel plates and the inner face of the aluminum can.

Four regions are used to represent the graphite reflector elements. The dimensions of the graphite are chosen to be the same as those of the fuel bearing region for a full element. The graphite is surrounded by a homogeneous mixture of carbon, water, aluminum, and void. The aluminum cans, and the water between the cans, are represented explicitly. The remaining three compositions in the reflector represent the graphite thermal column, its aluminum sleeve, and water which is present to the exterior of the graphite elements.

A printout of a sample PDQ mesh for the semi-permanent core configuration is shown in Fig. 4. The code allows for only 58 columns of the picture to be printed so that the graphite thermal column and its aluminum sleeve are not shown. The number densities and description for each PDQ region are given in Table 2.

3. Core Representation for PDQ in Cylindrical (R,Z) Geometry. The core and reflector materials are represented in cylindrical geometry by the use of five compositions. The core is represented in this geometry as a homogeneous region with an active height of 23.625 inches and an equivalent radius of 7.728 inches. The equivalent radius is based on a core cross sectional area equal to the number of elements times the cross sectional area per element, i.e. 19 x 3.189 in. x 3.035 in. The core is surrounded in the radial direction by a homogeneous region representing

TABLE 2

PDQ COMPOSITION DESCRIPTIONS IN RECTANGULAR GEOMETRY

PDQ Comp no.	Composition Description	Composition Volume Weighted Densities ($\times 10^{-24}$/cm^3)
1	reflector water exterior to graphite elements and between South face of core and thermal column	N_{H2O} = 0.033371
2	graphite thermal column	N_C = 0.0803
3	aluminum sleeve on thermal column	N_{AL} = 0.060453
4	water associated with graphite reflector elements	N_{H2O} = 0.033371
5	aluminum cans housing reflector elements	N_{AL} = 0.060453
6	carbon-aluminum-water-void mixture in graphite reflector element	N_C = 0.034072 N_{AL} = 0.006932 N_{H2O} = 0.013976
7	carbon associated with reflector element	N_C = 0.0803
8	core water	N_{H2O} = 0.033371
9	aluminum cans housing fuel elements	N_{AL} = 0.060453
10	aluminum-water mixture representing fuel plate edges and water between fuel region and aluminum can	N_{H2O} = 0.024694 N_{AL} = 0.015720
11	water-aluminum-uranium mixture representing fuel region for elements containing 17.85 gms of U-235 per plate	N_{235} = 0.00018199 N_{238} = 0.0000125 N_{AL} = 0.018146 N_{H2O} = 0.023220
12	water-aluminum-uranium mixture representing fuel region for elements containing 15.86 gms of U-235 per plate	N_{235} = 0.0001618 N_{28} = 0.0000111 N_{AL} = 0.018173 N_{H2O} = 0.023220
13	aluminum-water mixture for "dummy" plate edge and water in "glory holes"	N_{AL} = 0.024107 N_{H2O} = 0.020064
14	aluminum-water mixture for "dummy" plate and water in "glory holes"	N_{AL} = 0.028199 N_{H2O} = 0.017804
15	aluminum-water mixture for "dummy" plate and water in element C-4	N_{AL} = 0.018389 N_{H2O} = 0.023220

the graphite reflector elements. The thickness of this region is also determined from the area of the eleven graphite elements. The final region represented in the radial direction, starting from the core centerline outward, is reflector water.

In the axial direction beyond the core at top and bottom is an aluminum-water mixture representing non-fuel bearing sections of the plates, aluminum cans and water. Immediately adjacent to the aluminum-water mixture at the bottom of the core is another aluminum-water mixture representing the bottom grid plate and water. The top and bottom most region in the axial direction is water. The core and reflector components as defined in R-Z coordinates are shown in Fig. 5.

B. One-dimensional WANDA-IV Model and Geometrical Representation

The one-dimensional time independent group diffusion equations are solved in either radial or slab geometry by use of the WANDA-IV[4] code. The group diffusion equations are essentially of the same form as Eqn. 1 with the exception that the transverse buckling may be specified in one of several ways. These ways include: (1) group independent value by composition; (2) group dependent value by composition and (3) group dependent value by point. The boundary condition at interfaces between adjacent regions is that the net current is continuous. No boundary condition is placed on the flux at such interfaces. At external boundaries, either

the net current or flux may be set equal to zero; the net current must be zero at R equal to zero in radial geometry.

The core and reflector materials are represented in either radial or axial slab geometry in the same manner as for the two-dimensional R-Z model. In radial geometry starting from R equal to zero and proceding outward, the compositions are core, graphite reflector elements, and water. In axial slab geometry proceding from Z equal to zero downward the region designations are water, aluminum-water mixture, core, two aluminum-water regions, and water.

C. Neutron Spectrum Representation

The neutron energy spectrum is divided into four broad groups consistent with the maximum number allowable in both the PDQ and WANDA calculations. While the group boundary points are somewhat arbitrary, those chosen tend to minimize the restrictions placed on the group-diffusion equations as represented in the codes. Therefore, the lethargy width of the intermediate groups is chosen sufficiently large so that cross coupling between non-adjacent groups is minimal. It is assumed that the effects of upscattering from thermal energies to those above the upper energy of the thermal group can be neglected. The upper and lower energies for the groups chosen are listed in Table 3. This group structure is essentially the same as that used in the analysis of thermal reactors at both the Bettis Laboratory and the Knolls Atomic Power Laboratory.

TABLE 3

BROAD GROUP STRUCTURE

Group	Upper Energy (ev)	Lower Energy (ev)
1	10^7	0.821×10^6
2	0.821×10^6	5.53×10^3
3	5.53×10^3	0.683
4	0.683	0

Each of these broad groups, as defined in Table 3, is characterized by certain physical processes and is discussed in turn. In Group 1, the hydrogen cross section decreases rapidly with energy. As a consequence, inelastic scattering with oxygen, uranium, and aluminum make up a significant portion of the removal cross section from this group for the University of Maryland core. Due to the relatively inefficient slowing down properties in this energy range, the major portion of the fast neutron leakage occurs in this group. Finally about 75% of the fission neutrons appear, or are born, in Group 1.

The remaining 25% of the fission neutrons are born in Group 2. This group is characterized by low capture cross sections and a hydrogen scattering cross section which increases to about 20 barns at the lower cut-off point[5]. This higher hydrogen scattering cross section at the lower energies in the group is the main contribution to slowing down out of the group.

The hydrogen scattering cross section remains essentially constant in Group 3. In this energy range only minor perturbations from an inverse energy, 1/E, flux occur due to

a small amount of resonance absorption.

The main physical processes occurring in the thermal group are the rapid increase in hydrogen scattering cross section with decreasing energy and the higher absorption cross sections of this range. The absorption cross sections for the elements present in the University of Maryland core essentially follow an inverse velocity, 1/v, law in this energy range with some deviation occurring for U-235 and U-238.

D. Cross Sections for Fast Energy Groups

1. Fast Spectrum Approximations. The cross sections averaged over each of the first three groups in Table 3 were obtained using the GAM-1[6] code as programmed for the IBM 7090. Two methods, which are included as options in the code, were used to calculate approximate spectra and the associated group averaged cross sections. These methods are the volume integrated P-1 and the Fourier transform B-1 approximations as derived for a finite bare core from the time-independent Boltzmann equation with a volume isotropic source. The assumption of a bare core is not necessary in the P-1 approximation but it is assumed in this analysis. A brief outline of the methods is given below stating the other major assumptions necessary to obtain the desired equations.

The P-1 relations are obtained using a P-1 spherical harmonics expansion of the energy dependent angular flux. Therefore, the flux is assumed to be isotropic. The spatial

dependence of the resulting pair of equations is removed by integrating both the P-0 and the divergence of the P-1 equation over the region of interest. The finiteness of the core is accounted for by a leakage term, which for the bare core approximation is equal to the negative of the core buckling. This leakage term, or factor, can be specified as either energy dependent or energy independent.

In both the P-1 and B-1 methods, a Legendre polynomial expansion of the transference function, i.e. the cross section for changing the energy E' and direction $\vec{\Omega}'$ of a neutron into unit energy interval at E and unit solid angle around $\vec{\Omega}$, is performed in terms of the scattering angle of the neutrons. The addition theorem is then used to express the scattering angle in terms of the initial and final directions of the scattered neutron. After integration over the azimuthal angle, the Fourier transform of the resulting form of the one-dimensional transport equation is then taken in the B-1 method. This effectively suppresses the spatial dependence of the transport equation. When the Fourier transform of the wave equation is also taken, it is seen that the transform variable is equal to the square root of the buckling of the system. The angular flux in the transformed equations, actually the Fourier transform of the angular flux, is then expanded in Legendre polynomials. In the B-1 approximation, it is assumed that scattering is linear in angle in the laboratory system. Therefore, the B-1 approximation is obtained by assuming that only

the first two coefficients in the expansion of the transference function exist with the non-linear coefficients being set to zero. The leakage factor, which is the square root of the buckling for the B-1 approximation, can be specified only by an energy independent value.

The equations in either the P-1 or B-1 methods are solved successively by the code in each of 68 energy groups. In this manner, approximate spectra for the neutron flux and divergence of the current are obtained in the P-1 method whereas Fourier transform values of the flux and current spectra result if the B-1 method is used. Microscopic cross sections for the individual isotopes present in a region, as well as macroscopic cross sections for the homogenized region, are then averaged over the neutron flux spectrum for the energy groups defined in Table 3. The code accounts for spatial self-shielding of U-238 and determines the effective resonance integral for this isotope. The diffusion coefficient for each broad group is defined according to Fick's law.(6)

2. Method for Obtaining Fast Group Cross Sections for Core and Reflector Compositions. An average core spectrum was determined in order to calculate macroscopic cross sections for the above thermal groups for the material compositions present in the core. In order to obtain an average core spectrum, all the materials present in the core were homogenized into one region. GAM calculations were then performed for the homogenized mixture using the desired method. The leakage factors used were obtained from hand calculations for the initial GAM cases and from PDQ calculations for the final GAM calculations.

The average core spectra resulting from these calculations were then used in accordance with an additional option present in the GAM code. This option allows the calculated core spectrum, as well as the isotopic number densities for any desired material composition, to be used as input for further GAM calculations. The code then calculates the broad group macroscopic cross sections for the material composition by averaging over the input spectrum. In this manner macroscopic cross sections were obtained for each of the core compositions listed in Table 2.

It is not possible to calculate the diffusion coefficient for each material composition by the above method. The reason for this is that the GAM code uses both current and flux spectra in calculating the diffusion coefficient. When a flux spectrum is used as input for a GAM calculation, no current spectrum is calculated and a zero diffusion coefficient results. To circumvent this problem the diffusion coefficients were calculated in a manner discussed by Weinberg and Wigner,[7] and Pomraning.[8] This essentially consists of a parallel average of the transport cross section with respect to the flux spectrum. To accomplish this the diffusion coefficient was obtained as a function of energy for each material composition. The group averaged diffusion coefficient was then calculated for each material composition by averaging over the flux spectrum using the equation

$$D_i^j = \frac{\int_{i3} \frac{1}{\Sigma_{TR}^j(E)} \phi(E)d(E)}{\int_i \phi(E)dE} \qquad (3)$$

where:

D_i^j = average diffusion coefficient for ith energy group and jth material composition

$\sum_{TR}^{j}(E)$ = energy dependent transport cross section as a function of energy

$\phi(E)$ = neutron flux as a function of energy

Microscopic transport cross sections for each isotope were obtained for each of 68 energy groups from the same GAM calculations that yielded the average core spectrum. These microscopic values were then weighted by the volume weighted number densities to obtain the energy dependent macroscopic transport cross sections for each composition. The diffusion coefficient is then obtained using these values in a numerical integration of Eqn. 3. The assumption is explicitly made in this definition of the diffusion coefficient that the spectrum is separable in space and energy. This assumption is implicit in the B-1 and P-1 approximations so that no inconsistency occurs.

Fast group cross sections for the reflector materials were obtained in much the same manner as the core cross sections. The reflector water and graphite thermal column, therefore compositions 1 and 3 in Table 2, were considered separately, and their corresponding cross sections were obtained directly from GAM calculations performed for each region separately. The reflector elements were homogenized in the same manner as the core. An average spectrum was obtained, and then the procedure used for the core compositions was followed for those compositions associated with

the reflector elements. The leakage factors used for the reflector GAM calculations were chosen to be -1×10^{-6} cm^{-2} for the P-1 method and 1×10^{-3} cm^{-1} for the B-1 method. This choice is arbitrary as is also the assumption of a volume source in the reflector region. However, as is pointed out in Ref. 15, reflector constants using a relatively small leakage factor and a volume source appear to be satisfactory for reactors of the approximate size of the University of Maryland core.

E. Thermal Group Cross Sections

1. Thermal Spectra Approximations. Two methods of obtaining thermal spectra and associated cross sections were used to calculate multiplication constants for comparison with experiment for the semi-permanent core configuration. These are the well known Maxwellian[9] and Wigner-Wilkins[10] spectrum models as programmed in the TEMPEST II[11] code for the IBM 7090.

In the Maxwellian spectrum model, the neutrons are assumed to be in thermal equilibrium with the nuclei of the infinite non-absorbing surrounding medium. The energy distribution of the neutrons is determined by the temperature distribution of the moderator. The material composition of the region has no effect on the neutron spectrum which is given by the gas equation of Maxwell.

The Wigner-Wilkins method consists of converting a neutron conservation integral equation to a second order differential equation which is then solved by the TEMPEST code

to obtain a neutron flux spectrum. The integral equation is derived by considering the physical processes governing the velocity distribution of neutrons. The assumption is made initially that an infinite absorbing medium exists which is uniformly filled with slowing down material. Chemical binding of the atoms in the moderator is ignored. The assumption is then made that the moderator is a gas whose atoms have a Maxwellian energy distribution, as well as a constant scattering cross section independent of the velocity of the neutrons. Then the total number of neutrons acquiring a velocity in $d\vec{v}$ about $\vec{v}$ is equated to the losses out of this differential velocity element due to absorption and scattering. In the case of zero absorption, the resulting integral equation is satisfied by the Maxwellian distribution. This fact along with the principle of detailed balance is then used to obtain the final form of the integral equation which then yields the number of neutrons per CM^3 as a function of velocity.

In the neutron conservation integral equation, a kernel is used to represent the probability that a neutron of velocity $\vec{v}_1$ is scattered into $d\vec{v}$ about $\vec{v}$. In addition, the loss due to scattering out of the differential velocity element is dependent on the probability of a collision between a neutron of velocity $\vec{v}$ and a moderator atom with a Maxwellian velocity distribution. The integral equation is then converted into the previously mentioned second order differential equation using the additional assumption that the moderator gas is composed of hydrogen atoms which simplifies the kernel considerably.

2. Regionwise Thermal Cross Sections. Thermal cross sections for each of the compositions in Table 2, with the exception of the aluminum cans, were obtained directly from TEMPEST calculations performed for each composition. With the additional exception of the fuel regions, the various compositions were homogenized by volume weighting the elements present in the particular composition. The macroscopic cross sections were then averaged over the spectrum as calculated by the TEMPEST code. The diffusion coefficient was averaged directly by the code over the spectrum.

The aluminum cans were assumed to have the same spectrum as the surrounding water regions. The macroscopic absorption cross section and diffusion coefficient were then calculated for these regions based on the corresponding microscopic absorption and transport cross sections obtained from the TEMPEST calculations.

The treatment of the fuel regions takes a somewhat different form. This is due to the variation in the thermal flux that occurs in traversing from fuel to water in these regions. The fuel region isotopic number densities were flux and volume weighted to account for the variation in thermal flux according to the equation:

$$N_j = \sum_i N_j^i V^i \frac{\bar{\phi}^i}{\bar{\phi}_{cell}} \qquad (4)$$

where:

N_j^i = number density for jth isotope in the ith region

V^i = volume fraction of ith region in the cell

$\bar{\phi}_i$ = average thermal flux in the ith region

$\bar{\phi}_{cell}$ = average thermal flux in the cell

These volume and flux weighted values were used as input to TEMPEST for the fuel regions and the appropriate spectrum averaged cross sections were obtained.

3. Flux Weighting Factors. A three region P-3 approximation to the one-dimensional, time independent, and one velocity transport equation was performed by hand to obtain the flux weighting factors in Eqn. 4. The three regions in the calculation were the uranium-aluminum fuel, aluminum cladding and water. The one-dimensional coordinate system starts at the centerline of the fuel and extends through the aluminum cladding to the centerline of the adjacent water region. The calculation was only performed for the fuel regions with 16 grams of U-235 per plate. The assumption was made that these same factors hold for the 18 gram plate regions.

The derivation of the P-3 equations has been discussed extensively by several authors.[9,12,13] First the scattering kernel is expanded in Legendre polynomials in terms of the scattering angle. After use of the addition theorem and integration over the azimuthal angle, the angular flux is expanded in terms of Legendre polynomials. Then using the orthogonality properties of Legendre polynomials the P_N equations are obtained. The P_N equations are then truncated in the P-3 approximation so that only the first four moments in the expansion of the angular flux are

assumed to exist. For simplicity, only the first two coefficients in the expansion of the scattering kernel are allowed. Then the P-3 equations for the ith region, assuming no source is present for simplicity, are: (13)

$$\frac{dF_1^i(x)}{dx} + \Sigma_t^i \left(1 - \frac{\Sigma_{SO}^i}{\Sigma_t^i}\right) F_0^i(x) = 0$$

$$2\frac{dF_2^i(x)}{dx} + \frac{dF_0^i(x)}{dx} + 3\Sigma_t^i \left(1 - \frac{\bar{\mu}_0^i \Sigma_{SO}^i}{\Sigma_t^i}\right) F_1^i(x) = 0 \qquad (5)$$

$$3\frac{dF_3^i(x)}{dx} + 2\frac{dF_1^i(x)}{dx} + 5\Sigma_t^i F_2^i(x) = 0$$

$$3\frac{dF_2^i(x)}{dx} + 7\Sigma_t^i F_3^i(x) = 0$$

Where:

F_n^i = nth moment of flux for ith region

Σ_t^i = total cross section for ith region

Σ_{SO}^i = total scattering cross section of ith region

$\Sigma_{S1}^i = \bar{\mu}_0^i \Sigma_{SO}^i$ where $\bar{\mu}_0$ is the average cosine of the scattering angle.

Eqns. 5 were then solved for each region. The aluminum and fuel regions were assumed to be source free while a uniform isotropic source was assumed in the water region. Therefore the first of Eqns. 5 is equated to a source term, which is not a function of position, in the moderator region.

The solution to these equations proceeds in the same manner as given by Murray,[13] i.e. a solution is assumed to exist of the form:

$$F_n^i(x) = F_{nm}^i e^{\sum_t^i k_m^i x} \tag{6}$$

After substitution of Eqn. 6 into Eqns. 5 the k_m^i's were determined by solving the determinant of the coefficients of the set of homogeneous equations for each region. This yields a quadratic expression in k_m^{i2} so that

$$k_m = \pm \left[\frac{-b \pm (b^2 - 4c)^{\frac{1}{2}}}{2} \right]^{\frac{1}{2}} \tag{7}$$

where the region index has been suppressed and

$$b = \frac{27 \dfrac{\bar{\mu}_0 \Sigma_{s0}}{\Sigma_t} \left(1 - \dfrac{\Sigma_{s0}}{\Sigma_t} \right) + 55 \dfrac{\Sigma_{s0}}{\Sigma_t} - 90}{9} \tag{8}$$

$$c = \frac{105}{9} \left[\frac{\Sigma_{s0}}{\Sigma_t} \left(\frac{\bar{\mu}_0 \Sigma_{s0}}{\Sigma_t} - \bar{\mu}_0 - 1 \right) + 1 \right]$$

As is seen from Eqn. 7, four values of k_m result for each region with $k_2 = -k_1$ and $k_4 = -k_3$. Then the solution for each moment of the flux is given by

$$F_n^i(x) = \sum_{m=1}^{4} F_{nm}^i \, e^{k_m^i \sum_t^i x} \tag{9}$$

In addition to the values of k_m a set of coupling coefficients relating the arbitrary coefficients, i.e. the F_{nm}'s, was obtained by the substitution of Eqn. 9 into Eqns. 5. Again suppressing the region index these are given by:

$$r_{1m} = \frac{F_{1m}}{F_{0m}} = \frac{1}{k_m}\left(\frac{\Sigma_{s0}}{\Sigma_t} - 1\right)$$

$$r_{2m} = \frac{F_{2m}}{F_{0m}} = \frac{3\left(\frac{\bar{\mu}_0\Sigma_{s0}}{\Sigma_t} - 1\right) r_{1m} - k_m}{2k_m} \qquad (10)$$

$$r_{3m} = \frac{F_{3m}}{F_{0m}} = -\left(\frac{2k_m r_{1m} + 5r_{2m}}{3k_m}\right)$$

At the centerline of the fuel region (x = 0) and at the centerline of the moderator region (x = c) the boundary conditions are that the odd moments and derivatives of the even mements are zero. The moments of the flux are continuous at the fuel to cladding (x = a) and the cladding to water (x = b) interfaces. Upon using boundary conditions at the centerline of the fuel region and after manipulation the equations for the moments in the fuel region become:

$$F_0^U(x) = M_{01}^U \cosh k_1^U \Sigma_t^U x + M_{03}^U \cosh k_3^U \Sigma_t^U x$$

$$F_1^U(x) = r_{11}^U M_{01}^U \sinh k_1^U \Sigma_t^U x + r_{13}^U M_{03}^U \sinh k_3^U \Sigma_t^U x$$

$$F_2^U(x) = r_{21}^U M_{01}^U \cosh k_1^U \Sigma_t^U x + r_{23}^U M_{03}^U \cosh k_3^U \Sigma_t^U x \qquad (11)$$

$$F_3^U(x) = r_{31}^U M_{01}^U \sinh k_1^U \Sigma_t^U x + r_{33}^U M_{03}^U \sinh k_3^U \Sigma_t^U x$$

where U denotes the fuel region. The equations for the moments in the cladding become (with C denoting aluminum cladding):

$$F_0^C(x) = M_{01}^C \cosh k_1^C \Sigma_t^C x + M_{02}^C \sinh k_1^C \Sigma_t^C x$$
$$+ M_{03}^C \cosh k_3^C \Sigma_t^C x + M_{04}^C \sinh k_3^C \Sigma_t^C x$$

$$F_1^C(x) = r_{11}^C M_{01}^C \sinh k_1^C \Sigma_t^C x + r_{11}^C M_{02}^C \cosh k_1^C \Sigma_t^C x$$
$$+ r_{13}^C M_{03}^C \sinh k_3^C \Sigma_t^C x + r_{13}^C M_{04}^C \cosh k_3^C \Sigma_t^C x \qquad (12)$$

$$F_2^C(x) = r_{21}^C M_{01}^C \cosh k_1^C \Sigma_t^C x + r_{21}^C M_{02}^C \sinh k_1^C \Sigma_t^C x$$
$$+ r_{23}^C M_{03}^C \cosh k_3^C \Sigma_t^C x + r_{23}^C M_{04}^C \sinh k_3^C \Sigma_t^C x$$

$$F_3^C(x) = r_{31}^C M_{01}^C \sinh k_1^C \Sigma_t^C x + r_{31}^C M_{02}^C \cosh k_1^C \Sigma_t^C x$$
$$+ r_{33}^C M_{03}^C \sinh k_3^C \Sigma_t^C x + r_{33}^C M_{04}^C \cosh k_3^C \Sigma_t^C x$$

The moderator equations contain a particular integral for the source term. The boundary conditions are applied at the moderator centerline ($x = c$) and the zeroeth moment of the flux is normalized to one at the clad-moderator interface ($x = b$). The moderator equations become (with

W denoting water):

$$F_0^W(x) = D_{01}^W\left[\cosh\ k_1^W\Sigma_t^W(x-c)-\cosh\ k_1^W\Sigma_t^W(b-c)\right]$$

$$+ D_{03}^W\left[\cosh\ k_3^W\Sigma_t^W(x-c)-\cosh\ k_3^W\Sigma_t^W(b-c)\right] +1 \qquad (13)$$

$$F_1^W(x) = r_{11}^W D_{01}^W \sinh\ k_1^W\Sigma_t^W(x-c) + r_{13}^W D_{03}^W \sinh\ k_3^W\Sigma_t^W(x-c)$$

$$F_2^W(x) = r_{21}^W D_{01}^W \cosh\ k_1^W\Sigma_t^W(x-c) + r_{23}^W D_{03}^W \cosh\ k_3^W\Sigma_t^W(x-c)$$

$$F_3^W(x) = r_{31}^W D_{01}^W \sinh\ k_1^W\Sigma_t^W(x-c) + r_{33}^W D_{03}^W \sinh\ k_3^W\Sigma_t^W(x-c)$$

In the above equations:

$$F_{01}^i = \frac{M_{01}^i+M_{02}^i}{2} \qquad F_{02}^i = \frac{M_{01}^i-M_{02}^i}{2}$$

$$F_{03}^i = \frac{M_{03}^i+M_{04}^i}{2} \qquad F_{04}^i = \frac{M_{03}^i-M_{04}^i}{2} \qquad (14)$$

$$D_{01}^W = \frac{M_{01}^W}{\cosh\ k_1^W\Sigma_t^W c} \qquad D_{03}^W = \frac{M_{03}^W}{\cosh\ k_3^W\Sigma_t^W c}$$

When the boundary conditions of continuity of the moments are used at the fuel to cladding and cladding to water interfaces, eight equations in eight unknowns are obtained. The constants used solving these equations are listed in Table 4.

TABLE 4

CONSTANTS FOR SOLUTION OF P-3 EQUATIONS

k_1	2.84256	2.07206	1.97620
k_3	1.13869	0.56913	0.103422
Σ_t (cm^{-1})	0.948114	0.093321	3.21691
r_{11}	-0.315918	-0.057528	-0.002673
r_{13}	-0.788640	-0.209445	-0.051091
r_{21}	-0.333292	-0.458354	-0.498624
r_{23}	0.538877	0.052012	0.002189
r_{31}	0.406029	0.407030	0.422305
r_{33}	-0.262977	-0.012684	-0.001208

The solution for the scaler flux in each region is:

$$F_0^U(x) = 0.580454 \cosh 2.695072\, x + 0.416140 \cosh 1.07961\, x$$

$$F_0^C(x) = 0.042332 \cosh 0.193367\, x + 0.061079 \sinh 0.193367\, x + 0.956427 \cosh 0.053112\, x + 0.0036399 \sinh 0.053112\, x$$

$$F_0^W(x) = -0.028468 \left[\cosh 6.35726\,(x-c) - 2.30509\right] - 1.33429 \left[\cosh 0.332699\,(x-c) - 1.002989\right] + 1 \qquad (15)$$

This solution is shown graphically in Fig. 6. The flux weighting factors for the uranium, aluminum cladding and water obtained by the integration of Eqns. 15 and normalized to the average flux in the cell are given in Table 5. The symbol $\bar{\phi}$ is used to denote the scaler flux in the table which is consistent with the nomenclature in Eqn. 4.

TABLE 5

P-3 FLUX WEIGHTING FACTORS

$\frac{\bar{\phi}^U}{\bar{\phi}_{cell}}$	$\frac{\bar{\phi}^C}{\bar{\phi}_{cell}}$	$\frac{\bar{\phi}^W}{\bar{\phi}_{cell}}$
0.97762	0.97976	1.00915

CHAPTER IV

ANALYSIS OF SEMI-PERMANENT CORE CONFIGURATION

The initial sets of calculations were done to investigate the ability of the various analytical models discussed in Chapter III to predict the core excess reactivity for the semi-permanent core arrangement of Fig. 1. This investigation was motivated by a desire to choose a suitable model to predict reactivity changes incurred in reactor experiments and core modifications.

A. Experimental Excess Reactivity

The calculations performed in this analysis were done assuming a core without control rods with the through and beam tubes flooded. It is necessary to have an estimate of the core excess reactivity for the semi-permanent core configuration under these conditions in order to make a comparison of the relative usefulness of the analytical models investigated. This is provided by data resulting from a series of experiments[1] performed by Drs. D. Duffey, J. Fisher, and Mr. A. Diaz in March and April of 1962. This data was obtained by inserting paraffin plugs in the beam and through tubes to simulate flooding of these facilities. The values for the measured control rod positions and excess reactivity obtained are given in Table 6.

The reactivity ρ defined by $(K_{eff} - 1)/K_{eff}$ was obtained using the control rod calibration curves given in Ref. 1 and reproduced in Figs. 7-9. An analysis of the data used in

TABLE 6

MEASURED REACTIVITY FOR SIMULATED FLOODING OF EXPERIMENTAL FACILITIES

Shim no. 1 cm	Shim no. 2 cm	Reg. Rod cm	Core Reactivity % ρ
43.95	45.98	0	0.988

obtaining these curves shows that the delayed neutron data of Hughes[14] was used. No correction for the finiteness of the core was made. The common practice in the analysis of experiments today is to use the later data of Keepin[14] which yields a delayed neutron fraction of .0065 for an infinite core fueled with U-235 as opposed to a value of .0075 using the data of Hughes. It is estimated in Chapter V, using Keepin's data, that the effective delayed neutron fraction for the University of Maryland reactor is .0078. The inhour equation can be written approximately as

$$\rho = \frac{K_{eff}^{-1}}{K_{eff}} = \frac{\ell^*}{TK_{eff}} + \gamma \sum_{i=1}^{6} \frac{\beta_i}{1+\lambda_i T} \qquad (16)$$

where:

ℓ^* = neutron lifetime

T = stable reactor period

β_i = delayed neutron fraction for ith delayed neutron group

λ_i = decay constant of ith group of delayed neutrons

$\gamma = \beta_{eff}/\beta$ = average correction for finiteness of core

From Eqn. 16, it is seen that core reactivity is proportional to the ratio of effective to infinite delayed neutron fractions if an average correction is assumed and if the stable period is sufficiently long so that the first term of the right hand side can be neglected. This amounts to a correction of approximately 3% so that the core excess reactivity, based on experiment, becomes about 1% or possibly 1.02% ρ .

Data obtained from Ref. 16 and Ref. 1 are used to ascertain the error associated with the measurement. Since the measurement was not repeated, only a rough estimate may be made of this uncertainty. In the material in Ref. 16 Dr. Fisher discusses a series of measurements made over a period of $1\frac{1}{2}$ years for the semi-permanent core configuration with the experimental facilities voided. The data from these measurements is partially reproduced in Table 7 along with that from Ref. 1.

TABLE 7

CORE EXCESS REACTIVITY WITH
EXPERIMENTAL FACILITIES VOIDED

Date	Shim no. 1 cm	Shim no. 2 cm	Reg. Rod cm	ρ (%)
4/16/62	46.02	45.96	33.80	0.703
9/17/62	47.99	47.99	34.94	0.534
9/7/63	48.00	48.00	24.60	0.630
5/23/64	48.00	48.00	26.35	0.613

If it is assumed that the reactivity worth of the experiment would remain the same then the uncertainty in the core reactivity in the experiment can be obtained from the variation in the unperturbed core reactivity. Therefore from

Table 7, the maximum error is seen to be .17%$\Delta\rho$. This variation is due to such things as temperature and the change over periods of time of console control rod dial positions relative to actual control rod positions. The above error estimate does not include such effects as control rod interaction, which are neglected.

B. Axial Buckling Calculation

As discussed in Chapter III, the group diffusion equations as programmed for the PDQ code require a value of the group independent transverse, or vertical, buckling to be specified as input for the X-Y calculations. This axial buckling value is spatially and energy independent as is seen from Eqn. 1. Therefore the same value of the axial buckling is assumed to hold in the reflector regions as well as in the core regions.

1. Cylindrical Core Method. Two methods were used to obtain a value of the axial buckling. These methods were chosen because they tend to minimize eigenvalue differences between one and two dimensional problems.

In the first of these methods the core was cylindricized for an R-Z calculation as shown in Fig. 5 and discussed in Chapter III. To obtain input for this calculation a preliminary PDQ calculation was performed in X-Y coordinates. The preliminary X-Y calculation utilized Wigner-Wilkins thermal cross sections and fast group cross sections using the P-1 model. Core averaged macroscopic cross sections and diffusion coefficients for the R-Z calculation were obtained by flux and area weighting the cross sections

over the core proper using the equations

$$\bar{D}_i = \frac{\int D_i(\vec{r})\,\phi_i(\vec{r})\,dA}{\int \phi_i(\vec{r})\,dA} \qquad \bar{\Sigma}^A_i = \frac{\int \Sigma^A_i(\vec{r})\,\phi_i(\vec{r})\,dA}{\int \phi_i(\vec{r})\,dA}$$

$$\bar{\Sigma}^R_i = \frac{\int \Sigma^R_i(\vec{r})\,\phi_i(\vec{r})\,dA}{\int \phi_i(\vec{r})\,dA} \qquad \overline{\nu\Sigma^f_i} = \frac{\int \nu\Sigma^f_i(\vec{r})\,\phi_i(\vec{r})\,dA}{\int \phi_i(\vec{r})\,dA} \qquad (17)$$

where i denotes the energy group number and the integrations were carried out over the core proper. The symbols have the same definitions as given previously. The reflector elements were homogenized in the same manner as the core components. P-1 GAM and Wigner-Wilkins TEMPEST calculations were performed for the aluminum water mixtures while the reflector water cross sections were taken to be the same as in the X-Y calculations. The input cross sections are given by energy group and composition in Appendix A. The core multiplication constant obtained as output of the calculation was 1.0231.

A series of one dimensional radial WANDA calculations for the cylindricized core were performed for a slice through the center of the core using several axial bucklings. The axial bucklings were supplied as energy and spatially independent values. The input cross sections for core, reflector elements and reflector water were the same as for the corresponding PDQ compositions given in Appendix A. A curve was then drawn plotting the resulting multiplication constant versus input buckling.

These data are shown in Fig. 10 and listed in Table 8. It may be seen from the data that the axial buckling value of 0.0016 cm^{-2} in the radial calculations gave the same K_{eff} as the R-Z calculation of Section IV-A.

TABLE 8

ONE-DIMENSIONAL RADIAL WANDA RESULTS

Input B_Z^2 cm^{-2}	Core k_{eff}
0	1.1077
0.0016	1.0230
0.00175	1.0156

2. Axial Slab Method. In the above cylindrical core method a gross approximation must be made regarding the core, i.e. that the core may be cylindricized. However, it has the advantage that a transverse buckling value is obtained which is used in a consistent manner in the X-Y calculations. Additionally, this method makes no further assumptions with regard to the shape of the flux in the top and bottom reflectors.

Such assumptions must be considered in the second method investigated. In this case, the axial buckling was obtained from one dimensional axial slab calculations. The core geometry used is the same as shown in Fig. 5 for a vertical slice through the core. The input cross sections are the same as used in the R-Z calculations for the corresponding compositions. Energy dependent values of the radial or X-Y bucklings for the core were obtained from the preliminary PDQ calculation by integrating the

group diffusion equations over the core area. Therefore the group dependent bucklings were defined by

$$\bar{B}_i^2[X,Y] = \frac{-\int \nabla \cdot [D_i(\vec{r}) \nabla \phi_i(\vec{r})] dA}{\int D_i(\vec{r}) \phi_i(\vec{r}) dA} \qquad (18)$$

where $\bar{B}_i^2[X,Y]$ = average X-Y buckling for ith energy group.

The integrations are carried out over the core proper and the other symbols have the same meaning as defined in Chapter III. Eqn. 18 can be written in equivalent form as:(15)

$$\bar{B}_i^2[X,Y] = \frac{\int \left[\chi_i \sum_{i=1}^{4} \frac{\nu \Sigma_i^f(\vec{r})}{\lambda} \phi_i(\vec{r}) + \Sigma_{i-1}^R(\vec{r}) \phi_{i-1}(\vec{r}) \right] dA}{\int D_i(\vec{r}) \phi_i(\vec{r}) dA} \qquad (19)$$

$$- \frac{\int [\Sigma_i^R(\vec{r}) + \Sigma_i^A(\vec{r}) + D_i(\vec{r}) B_Z^2] \phi_i(\vec{r}) dA}{\int D_i(\vec{r}) \phi_i(\vec{r}) dA}$$

The group dependent radial (X,Y) bucklings were obtained using Eqn. 19 and are listed in Table 9.

TABLE 9

GROUP DEPENDENT RADIAL (X,Y) BUCKLINGS FOR DETERMINATION OF AXIAL BUCKLING

Energy Group	Buckling B^2 X,Y cm^{-2}
1	0.012201
2	0.008355
3	0.005736
4	-0.003032

The negative buckling in Group 4, i.e. the thermal energy group, is caused by fast neutrons being slowed down to thermal energies in the reflector and returning to the core.

The specification of a transverse (X,Y) buckling in the top and bottom reflector regions is somewhat arbitrary. This is because the shape of the flux in these regions is not precisely known. At the core-reflector interfaces, one could reasonably assume that the reflector flux shape would be similar to that in the adjacent core regions. At large distances from the core-reflector interface one would expect the flux shape to be more nearly flat; for an infinite reflector the X-Y buckling in the reflector would approach zero at large distances from the core.

Since reflector neutrons further than a few mean free paths from the core have little effect, it was assumed in this analysis that the buckling used in the reflector was the group independent core value. This was obtained by using an equivalent bare core model and data from the preliminary X-Y PDQ calculation. In this model, the group diffusion equations are integrated over the core. After defining the group dependent buckling as in Eqn. 18 and making this substitution each term is multiplied and divided by the core integrated flux. After dividing by the core area, the group diffusion equations may be written in terms of average quantities as

$$\bar{D}_i B_i^2 [X,Y] \bar{\phi}_i + \left[\bar{\Sigma}_i^A + \bar{\Sigma}_i^R + \bar{D}_i B_Z^2 \right] \bar{\phi}_i = \frac{\chi_i \sum_{i=1}^{K} \overline{\nu \Sigma_i^f} \bar{\phi}_i + \bar{\Sigma}_{i-1}^R \bar{\phi}_{i-1}}{\lambda} \qquad (20)$$

where ϕ_i is the core averaged flux for the ith group and the other terms are defined by Eqns. 17 and 18.

The solution to Eqn 20 is obtained for λ by solving the determinant of the coefficients of the fluxes. This gives the equation, with K_{eff} equal to λ :(21)

$$K_{eff} = \chi_1 \left[\frac{(1-p_1)(\eta f)_1}{L_1} + \frac{(1-p_2)p_1(\eta f)_2}{L_1 L_2} + \frac{(1-p_3)p_1 p_2(\eta f)_3}{L_1 L_2 L_2} + \frac{p_1 p_2 p_3(\eta f)_4}{L_1 L_2 L_3 L_4} \right] + \chi_2 \left[\frac{(1-p_2)(\eta f)_2}{L_2} \quad \frac{(1-p_3)p_2(\eta f)_3}{L_2 L_3} + \frac{p_2 p_3(\eta f)_4}{L_2 L_3 L_4} \right] \tag{21}$$

where:

$$p_i = \frac{\overline{\Sigma}^R_i}{\overline{\Sigma}^A_i + \overline{\Sigma}^R_i}$$

$$(\eta f)_i = \frac{\overline{\nu \Sigma}^f_i}{\overline{\Sigma}^A_i}$$

$$L_i = 1 + \frac{\overline{B}^2_i \overline{D}_i}{\overline{\Sigma}^A_i + \overline{\Sigma}^R_i} \qquad \text{where } \overline{\Sigma}^R_i = 0 \text{ for } i = 4$$

$$\overline{B}^2_i = \overline{B}^2_i[X,Y] + B^2_Z$$

The group independent buckling was obtained by assuming that the group bucklings were constant, i.e. $\overline{B}^2_i = \overline{B}^2$, and solving

Eqn. 21 numerically. The value of the group independent X-Y buckling obtained in this manner was 0.00675 cm^{-2}.

The K_{eff} from the axial WANDA calculation performed with the regionwise bucklings defined as above was 1.0132. The method to obtain the group independent axial buckling was to solve, again numerically, Eqn. 21 for the value that gave the calculated K_{eff}. The X-Y bucklings were the values used as input in the WANDA calculation. A curve of K_{eff} versus axial buckling was drawn to determine the value as shown in Fig. 11. The value of the axial buckling corresponding to the calculated K_{eff} was found to be 0.00169 cm^{-2}.

The values obtained by both the cylindrical core and axial slab methods agreed reasonably well. It was estimated from Fig. 10 that the difference in K_{eff} due to the difference in calculated axial buckling would be approximately 0.5%ΔK. The value selected for the PDQ calculations was that obtained from the R-Z PDQ and the radial WANDA calculations. The choice is again arbitrary but if the effects of cylindricizing the core are neglected, this method is more satisfying.

The second method, i.e. the axial slab method, should really consist of an iterative procedure. Thus the axial buckling found above should be used as input into a second X-Y PDQ calculation. Then the output from this calculation should be used in a new axial calculation. This procedure would then continue until a minimum difference in K_{eff} between the two-dimensional and one-dimensional calculations

was obtained. This procedure would be quite time consuming with respect to computer time and so it was not carried further. In view of the uncertainty as to the proper choice of reflector buckling to be used, it was felt that the additional computer time required would not be justified. In addition, the change in the calculated K_{eff} due to an iterated axial buckling would only be on the order of a tenth of a percent.

C. Comparison of Fast Energy Group Methods

1. General Description of Calculations. In the comparison of the fast energy group analytical models, the thermal group cross sections were obtained using the Wigner-Wilkins model as described in Chapter III. These cross sections are tabulated in Fig. 4 and were kept constant throughout the analysis discussed in this section. Two-dimensional PDQ X-Y calculations were then performed to determine reactivity differences using the cross sections for the above thermal energy groups as calculated with the volume integrated P-1 and Fourier transform B-1 methods.

Fast group core cross sections were obtained using the P-1 method for two distinct cases. These consisted of calculating core spectra, using both energy dependent and energy independent buckling values to specify the leakage factors in the GAM calculations. The energy dependent values were calculated from the preliminary

PDQ using Eqn. 19. The energy independent buckling was taken to be an effective average fast group value. This value was calculated using Eqn. 21 where it was assumed that $\bar{B}_i^2 = \bar{B}^2$ for i = 1,2,3 and $\bar{B}_4^2$ was that value obtained using Eqn. 19. Thus an effective fast group value was calculated that would give the same multiplication constant as if the energy dependent values were used. The same energy independent value was used to specify the leakage factor for the B-1 calculation where in this case the leakage factor is the positive square root of the buckling. Both energy dependent and energy independent values are tabulated in Table 10.

TABLE 10

BUCKLINGS USED TO SPECIFY GAM LEAKAGE FACTORS

Energy Group	Energy Dependent Value cm^{-2}	Energy Independent Value cm^{-2}
1	0.013951	0.0112
2	0.010105	0.0112
3	0.007486	0.0112

The resulting core spectra were then used to obtain regionwise cross sections for the core materials as discussed in Chapter III. The cross sections for the energy groups above 0.683 ev are tabulated, for the core compositions, in Appendices B and C for the P-1 calculation using the energy dependent leakage factors and the B-1 calculation using the energy independent leakage factor, respectively. The cross section data for the P-1 energy independent buckling calculation are shown in Fig. 4.

The reflector constants for the energy dependent P-1 calculation were exactly the same as those for the P-1 energy independent case and are shown in Fig. 4. The B-1 fast group constants for the reflector compositions are similar to the corresponding P-1 values so that they are not shown.

2. Results from Calculations Utilizing Various Fast Group Methods. The core multiplication constants from the PDQ X-Y calculations are listed in Table 11.

TABLE 11

CORE K_{eff} UTILIZING P-1 AND B-1 FAST GROUP CONSTANTS AND WIGNER-WILKINS THERMAL GROUP CONSTANTS

Fast Group Method	Buckling in GAM	Core K_{eff}
P-1	Energy Dependent	1.00740
P-1	Energy Independent	1.01048
B-1	Energy Dependent	1.01590

The total reactivity spread is less than 1% $\Delta\rho$ with the core eigenvalue obtained using the P-1 method with a group independent leakage factor experiencing the least deviation from the experimental value of 1.02% ρ. The difference in K_{eff} between the experimental result and this best result is only 0.02% $\Delta\rho$ which is fortuitous and probably the result of cancellation of errors. Usually the B-1 method should give the better results. This can best be understood by deriving the P-1 equations in the same manner as the B-1 equations, i.e. by using a Fourier

transform technique in slab geometry. If this is done, then it can be seen that the P-1 equations are in fact an approximation to the B-1 equations with the result that the energy dependent flux spectrum, as calculated using the B-1 method, should be more accurate. On the other hand, one would also expect the P-1 result using energy dependent bucklings to obtain the fast group cross sections to give better agreement with experiment than the P-1 result obtained using an energy independent buckling, since the gross core flux shape and leakage is supposedly better represented with energy in the former case.

There are several possible uncertainties and sources of error that affect the calculations. While a detailed analysis of such errors and uncertainties would be prohibitive, if not impossible, some of these are:

A. Inherent approximations of the theoretical methods.
B. Method of application of the theoretical methods.
C. Finite difference approach to solution and PDQ mockup.
D. Axial buckling uncertainty.
E. Cross section uncertainties.
F. Fuel loading uncertainties.

The reference to the finite difference approach means the sensitivity of an eigenvalue problem with regard to the PDQ mesh description. It is obvious for example, that the coarser the description of the core, the less accurate the calculation of the fluxes and eigenvalue will

be. In some instances, the choice of how to represent the core is questionable. For instance, the aluminum cans were represented explicitly. This was done through a desire to represent the slowing down source to the thermal group as accurately as possible as a function of position. On the other hand, diffusion theory is not accurate for regions that are thin compared with a mean free path.

The use of the theoretical methods is admittedly somewhat arbitrary. Thus the definition of an average core spectrum for energies above 0.683 ev is an approximation since the spectrum changes from point to point in the core. This is due to changes in the water to metal ratio as well as reflector effects near the core periphery. The treatment of each region thermally as a separate entity with its own particular spectrum, using the Wigner-Wilkins model, is also somewhat questionable. It is stated in Ref. 15 that the Wigner-Wilkins model is a good approximation for regions that are large compared to their mean free path which is true of the fuel regions. However, the combined thickness of the surrounding lightly absorbing regions, which all have essentially the same thermal spectrum, is only on the order of one mean free path.

It may be noted that if the value of axial buckling that was calculated in the one-dimensional slab treatment had been used, then the B-1 method would have given the best agreement with experiment. This was a matter of choice. However if the value obtained by the second

method, i.e. the axial slab method, had been used it would not diminish the uncertainty since it would be based on assumptions with regard to the treatment of the top and bottom reflectors as well as the actual use of a constant buckling value in core and reflector in the X-Y calculations.

The above are examples of the types of uncertainties that may occur due to judgement of how to use the theoretical models or how to define and calculate a quantity such as the transverse buckling. The remaining uncertainties are of the types that are incurred when it is assumed that a particular model will suffice to perform a detailed calculation, e.g., such as the assumption that diffusion theory will be adequate, or the practical type that must be incurred such as the neglect of impurities in core materials and the neglect of a loading uncertainty of $\pm$ 0.2 grams of U-235 per plate. Cross section uncertainties exist in that there are uncertainties in the measurement of these quantities, in addition to the type of error that may follow from a bad value on the library tapes. While a detailed check of the cross section libraries was not made some of the more important values, such as the thermal capture to fission ratio for U-235, were checked and agreed with other sources of data.[5,18]

In view of the above remarks, the agreement between the calculated K_{eff}'s and the experimental result is considered quite good. For purposes of comparison the significant core parameters, as calculated from the PDQ output for each calculation, are listed in Table 12.

TABLE 12

CORE AVERAGED PARAMETERS RESULTING FROM COMPARISON OF FAST GROUP METHODS

	P-1 Method$_2$ Variable B^2 in GAM	P-1 Method$_2$ Constant B^2 in GAM	B-1 Method$_2$ Constant B^2 in GAM
$(\eta f)_1$	0.6972	0.6837	0.6764
$(\eta f)_2$	1.3282	1.3292	1.3295
$(\eta f)_3$	1.2568	1.2576	1.2582
$(\eta f)_4$	1.4967	1.4969	1.4969
p_1	0.9938	0.9937	0.9935
p_2	0.9967	0.9967	0.9966
p_3	0.9506	0.9503	0.9501
τ_1	25.1002	25.2325	22.7706
τ_2	12.4619	11.7221	11.4687
τ_3	9.4056	9.2071	9.2193
L^2	9.0704	9.0676	9.0650
K_∞	1.4807	1.4807	1.4805

where:

$$\tau_i = \frac{\bar{D}_i}{\sum_i^A + \sum_i^R} \qquad \text{(for } i = 1,2,3\text{)}$$

$$L^2 = \frac{\bar{D}_4}{\sum_4^A}$$

and τ_i is the neutron age for the ith energy group above thermal energies, L^2 is the thermal diffusion area and K_∞ is the infinite multiplication factor. K_∞ is obtained by letting B_i^2 equal zero in the equivalent bare core multiplication formula (Eqn. 21). All other symbols are defined as in Eqn. 21.

Evidently, since the K_∞ values remain about constant, leakage variations account for the major differences in

the calculations utilizing the different methods. The neutron age (τ) shows this to be the case, especially for the B-1 calculation. A comparison of the Group 1 contributions to the neutron age, where most of the leakage occurs, shows the B-1 value to be about 10% lower than the corresponding P-1 values.

Another point worth noting from Table 12 is the relatively high thermal diffusion areas. This is partly due to the high aluminum content of the core and partly a consequence of representing the aluminum cans explicitly. Also the Wigner-Wilkins method classically overestimates thermal diffusion lengths[15]. These are to some extent, the reasons for the relatively small axial buckling which corresponds to a reflector savings of about 9 cm. Usually, measured values of reflector savings, for water, are quoted to be from 7.5 to 8.5 cm[17].

The explicit representation of the aluminum cans would seem to overestimate the thermal axial leakage in these regions. However, if the aluminum cans had been homogenized with water with a resulting lower core diffusion coefficient for thermal neutrons, then it would be expected from one group theory that the axial reflector savings would decrease and the axial buckling would increase. In other words the effects tend to cancel with respect to the core multiplication constant. There is little, if any, effect due to this representation in the X-Y direction, since these regions are thin.

D. Comparison of Thermal Group Methods

For the sake of completeness, a PDQ calculation using thermal cross sections averaged over an unhardened Maxwellian spectrum was performed to make a comparison of the effects on K_{eff} with the Wigner-Wilkins model. The fast group constants were the same as in the calculation performed with constants obtained from a P-1 calculation, with an energy independent leakage factor, using a constant GAM buckling of 0.0112 cm^{-2}. Thus the fast group constants were taken to be the same as shown in Fig. 4. The Maxwellian thermal group constants, that were used for each region, are shown in Appendix D. The composition descriptions are given in Chapter III and may be identified from Fig. 4.

The resulting core K_{eff} is given in Table 13 along with the result from the comparable PDQ calculation using Wigner-Wilkins thermal cross sections.

TABLE 13

COMPARISON OF CORE K_{eff} FOR WIGNER-WILKINS AND UNHARDENED MAXWELL-BOLTZMANN THERMAL SPECTRUM MODELS

	Maxwell-Boltzmann Thermal Spectrum	Wigner-Wilkins Thermal Spectrum
K_{eff}	1.0365	1.0105

The core K_{eff} resulting from the use of a Maxwell-Boltzmann unhardened spectrum is 2.6% ΔK higher than that obtained using the Wigner-Wilkins model. There are at least two

reasons for this difference.

First, in the method using unhardened Maxwell-Boltzmann thermal cross sections, the thermal absorptions in the regions surrounding the fuel regions make up a smaller fraction of the total thermal absorptions than in the calculation using the Wigner-Wilkins model. This is due to using a constant spectrum, which is only dependent on the moderator temperature in the Maxwellian model, as opposed to letting the spectrum vary according to the properties of the regions in the Wigner-Wilkins model. Thus for the Wigner-Wilkins model, the thermal spectrum is significantly softer in the water and aluminum-water regions where the absorption is small, than the thermal spectrum in the relatively high absorbing fuel regions. The net effect of letting the thermal spectrum vary according to the properties of the region is to increase the fraction of the thermal absorptions which take place in the regions surrounding the fuel regions, therefore to decrease the thermal utilization relative to the constant spectrum Maxwell-Boltzmann approximation.

The second reason for the difference in the calculated core K_{eff} from the two models is just the difference in the fuel region spectrums. Thus the Maxwellian model does not account for the preferential absorption of the neutrons at low energies. This preferential absorption has the tendency to shift the peak of the spectrum upward, thereby making the spectrum harder. Of course, if the cross

sections were 1/v, this would make no difference in the fission to absorption ratio. However the U-235 and U-238 cross sections deviate somewhat from a 1/v so that the effect is detectable.

The unhardened Maxwell-Boltzmann thermal spectrum model is useful because it predicts thermal diffusion lengths that agree well with experiment[15], as opposed to rather poor agreement with experimental diffusion lengths using the Wigner-Wilkins method. However, the unhardened Maxwell-Boltzmann model does not give good agreement with the value of the experimental reactivity for the University of Maryland Reactor.

E. Investigation of GAM Leakage Factors

The question naturally arises as to how sensitive the calculated core K_{eff} is to the GAM leakage factors. Thus, if the core energy dependent or energy independent bucklings were calculated from the PDQ results to be significantly different than the values that were used in the GAM calculations, an iterative process might be needed. This would necessitate the performance of a new set of GAM calculations, using the new buckling values, and then another set of PDQ's. This process would have to be repeated until convergence was obtained on the calculated core K_{eff}'s.

Initially, a check was made on the buckling values to determine the magnitude of the change for the PDQ calculations using P-1 constants obtained with both group

dependent and group independent leakage factors. Table 14 shows a comparison of the bucklings used in the GAM calculations with those obtained from the PDQ output.

TABLE 14

COMPARISON OF INPUT AND OUTPUT BUCKLINGS

	Energy Dependent Case		Energy Independent Case	
Energy Group	Input B^2 cm^{-2}	Output B^2 cm^{-2}	Input B^2 cm^{-2}	Output B^2 cm^{-2}
1	0.013951	0.013772	0.0112	0.0109
2	0.010105	0.009982	0.0112	0.0109
3	0.007486	0.007182	0.0112	0.0109

In the above table, the term input B^2 refers to the values obtained from the preliminary PDQ and used in the GAM calculations to obtain cross sections for the PDQ's, while output B^2 refers to those values calculated from the output of the PDQ calculations as discussed previously.

As can be seen from the table, there was some change in the buckling values. The reactivity change that would be experienced, if the previously mentioned iterative process was followed, was not known and had to be checked. Also, if the core K_{eff} was indeed sensitive to the leakage factors then an iterative process would be required in the analysis of the experiments.

The investigation of this question was carried out by performing additional calculations, with significantly different GAM bucklings, for the P-1 energy independent and B-1 spectrum models. The thermal cross sections for

the core and reflector regions, were consistent with the previous PDQ calculations using the Wigner-Wilkins thermal spectrum model. The fast group cross sections for the reflector regions were also consistent with the values that had been previously used. The buckling values chosen for the Gam calculations were 0.005 cm^{-2} and 0.014 cm^{-2} for the P-1 calculations. Only one additional PDQ calculation was performed using the B-1 method to obtain the cross sections for energies greater than 0.683 ev for the core regions. The GAM buckling chosen for this calculation was 0.005 cm^{-2}. The above thermal cross sections for the core regions, as obtained using the above quoted values for the core buckling and the different spectrum models, are tabulated in Appendices E, F and G.

The calculated PDQ core K_{eff}'s are listed in Table 15 along with the original values for comparison. The results are shown graphically in Fig. 12.

TABLE 15

INVESTIGATION OF K_{eff} WITH GAM INPUT BUCKLINGS

GAM Input B^2 cm^{-2}	P-1 Method K_{eff}	B-1 Method K_{eff}
0.005	1.01154	1.01339
0.0112	1.01048	1.01590
0.013951	1.00976	

The B-1 method is evidently somewhat more sensitive than the P-1 method with regard to the core K_{eff} obtained as a function of the core buckling used in the GAM calculations.

The core K_{eff} is shown to have a linear behavior as a function of the buckling, in Fig. 12 for the B-1 method, which is probably not the case. An estimate of the expected changes in K_{eff} that would be experienced if an iterative procedure were followed, can be obtained from the above data. From the last two results for the P-1 method, a coefficient in $\Delta K/\Delta B^2$ of -0.2617 cm^2 is obtained. Thus, if a new iteration was performed for a GAM buckling of 0.0109 cm^{-2}, the core K_{eff} should change by about +0.007% in ΔK_{eff} which is sufficiently small to be neglected. For the B-1 method, the coefficient in $\Delta K/\Delta B^2$ is +0.4848 cm^2 so that for the same change in buckling, the core K_{eff} should change by -0.012% ΔK_{eff}.

Some comments on Fig. 12 are in order. As can be seen from the figure, the two methods approach the same value of the multiplication constant for an infinite core, i.e. for a core with zero buckling, which is as it should be. For an extremely small core the two methods appear to diverge, though for the University of Maryland case the difference is still not very significant. The particularly slight slopes depicted in the K_{eff} versus B^2 curve should not be taken to mean that this would happen in, for example, a two group or perhaps a four group scheme with different energy group structure. In fact, the shallow slopes are a consequence of the four group scheme with a good representation of the few group spectrum which does not violate to extreme the physical constraints inherent in the group

diffusion method. This is discussed in some detail in Ref. 15, where it is shown for the P-1 method that the slope of K_{eff} versus core buckling increases significantly as the number of energy groups is reduced.

Care should be used, however, in which method to choose for a small core. Results can be misleading if, for example, the P-1 method was investigated on the basis of a large core and found to give good agreement with experiment. If the assumption was made that the same method was satisfactory for a small core the error could be significant.

In this particular case the P-1 method, using group independent bucklings for the GAM calculations, was chosen to use for the comparison between calculations and experiment performed in Chapter VI. This is because this method gave the best agreement with the experimental value of the core excess reactivity for the semi-permanent core configuration. While in the experiments, the core experienced considerable rearrangement, the core buckling does not vary by an amount that would cause concern.

CHAPTER V

EFFECTIVE DELAYED NEUTRON FRACTION

As has been discussed by several authors,[19,20] the effective delayed neutron fraction for a finite core is larger than the value for an infinite core. This is because the delayed neutrons have an average energy that is lower than that for prompt neutrons. This in turn means that their probability of escaping from the reactor is diminished somewhat compared to the probability of escape for prompt neutrons. Thus the effective delayed neutron fraction is somewhat larger for a finite core than the values for an infinite core.

This chapter is concerned with the calculation of the effective delayed neutron fraction (β_{eff}). This is necessary in order to make a comparison of the calculations with experiment.

A. Method 1

The delayed neutron fraction was calculated by two different methods. The first method, while relatively simple, has been found to give fairly good agreement with experiment.[20] This essentially consists of calculating ratios of the effective to infinite values of the delayed neutron fraction for each energy group. This is done using the ratio of fast non-leakage probabilities for delayed and prompt neutrons respectively. Thus, for

the ith delayed neutron group, this ratio is just

$$\frac{\beta_i(\text{eff})}{\beta_i} = \frac{1+\bar{B}^2 \tau_p}{1+\bar{B}^2 \tau_{iD}} \qquad (22)$$

where:

$\beta_i(\text{eff})$ = effective delayed neutron fraction for ith delayed neutron group

β_i = delayed neutron fraction for ith delayed neutron group for infinite core

$\bar{B}^2$ = average buckling value for above thermal energies

τ_p = average age of prompt neutrons

τ_{iD} = average age of ith group of delayed neutrons

The value of the buckling was calculated from the PDQ output for the P-1 energy independent case, using the equivalent bare core model as discussed previously. Thus the value of $\bar{B}^2$ was taken to be 0.0109 cm^{-2}.

The values of the prompt and delayed neutron ages were obtained from GAM calculations. The delayed neutron age, for the ith delayed neutron group, was obtained by assuming a unit source in the GAM energy group which corresponds closest to the quoted average value of the delayed neutron energy for the ith delayed neutron group. The energy group structure in GAM is such that in some cases, the same energy group was used for more than one delayed neutron group. The prompt age, i.e. the age for

prompt neutrons for the University of Maryland Reactor, was calculated to be 40.436 cm^2. The calculated ages for each group of delayed neutrons, as well as the average energy for each delayed neutron group, are tabulated in Table 16.

TABLE 16

DELAYED NEUTRON AGES

Delayed Neutron Group	GAM Average Energy Kev	Actual Energy Kev	τ_{iD} cm^2
1	269	250	14.183
2	568	560	19.172
3	443	430	16.094
4	443	420	16.094
5	620	730	22.257
6	568	515	19.172

No tabulated average energy could be found for the sixth delayed neutron group, so that it was assumed that the average energy for this group was the same as that for all the delayed neutrons.

The effective values of the delayed neutron fraction for each group were then calculated using Eqn. 22 and the above calculated values of the age for each delayed neutron group. The effective and infinite values of the delayed neutron fraction for each group are tabulated in Table 17, where the values for an infinite core are obtained from Ref. 14 using Keepin's delayed neutron data.

The value of the effective delayed neutron fraction from Table 17 is 0.0078. This value is obtained by summing the effective values over all delayed neutron

TABLE 17

EFFECTIVE DELAYED NEUTRON FRACTION

Delayed Neutron Group	β_i	$\beta_{i(eff)}$
1	0.000211	0.000263
2	0.001407	0.001680
3	0.001260	0.001544
4	0.002536	0.003108
5	0.000740	0.000858
6	0.000268	0.000334
Total	0.006422	0.007787

groups. This value is somewhat smaller, though in fairly good agreement, than quoted values from other sources (see Ref.20) for reactors of similar size and type. This could be due, at least in part, to the partial graphite reflector which makes the core appear larger than a corresponding completely water reflected core. The values usually reported are about 0.0080 to 0.0082 for the delayed neutron fraction of similar size cores.

There are certain assumptions that are made with this type of calculation. One of these is that it is assumed that the core buckling is precisely known for energies above 0.683 ev and that this can be represented by an average value using the equivalent bare core model. A second assumption is the neglect of the reflector as a source of delayed neutrons to the core. While the buckling value used is calculated in a manner to account for the reflector effects on the core average flux shape for energies greater than 0.683 ev, the ages for the delayed and prompt neutrons are calculated assuming a bare core with a volume fission source. This source

should actually be complemented by a source of neutrons from the reflector with a considerably different energy spectrum than that of the core fission spectrum.

However, in view of the fairly good agreement between the calculated number and other sources of data for similar size cores, the effects of the above assumptions on the calculated value of the effective delayed neutron fraction are assumed to be negligible. The above value of the effective delayed neutron fraction is the value that is used in the analysis of the experiments in Chapter VI.

B. Method 2

A second method was attempted to check the value calculated above. Unfortunately, an error was found after the calculation was performed, even though the calculated value agreed well with the above quoted value. However the calculation itself is of some interest so that a discussion of it is included. It is recommended that this method be investigated in future attempts to calculate an effective delayed neutron fraction using somewhat more sophisticated techniques than was used above.

In this method, the ratio of the effective delayed neutron fraction to that for an infinite core is calculated as shown by Henry[22] and other authors[20] from a PDQ calculation using the equation:

$$\gamma = \frac{\beta_{(eff)}}{\beta} = \frac{\sum_{n=1}^{2}\sum_{i=1}^{4} \nu\Sigma^{f}_{i,n}\int \phi_2^{+}(\vec{r})\,\phi_i(\vec{r})\,dA}{\sum_{n=1}^{2}\sum_{i=1}^{4} \nu\Sigma^{f}_{i,n}\left[\chi_1\int \phi_1^{+}(\vec{r})\,\phi_i(\vec{r})\,dA+\chi_2\int \phi_2^{+}(\vec{r})\,\phi_i(\vec{r})\,dA\right]} \qquad (23)$$

where ϕ_i^{+} = adjoint flux for ith energy group and n is summed over the two types of fuel regions in the core, i.e. the 18 and 16 gram per plate regions. The other quantities are defined previously.

The adjoint fluxes are obtained by performing an adjoint PDQ calculation. To obtain these values from the PDQ code entails considerable rearrangement. If the group diffusion equations are written in matrix form then, as shown by Weinberg and Wigner,[7] the adjoint equations can be obtained by transposing the matrix of the coefficients and replacing the column vector of fluxes by their adjoints. For a uniform core, the adjoint equations then become, neglecting the axial buckling term since it is self adjoint:

$$-D_4(\vec{r})\nabla^2\phi_4^{+}(\vec{r})+\Sigma_4^{A}(\vec{r})\,\phi_4^{+}(\vec{r}) = \chi_1\frac{\nu\Sigma_4^{f}(\vec{r})}{\lambda}\phi_1^{+}(\vec{r}) + \chi_2\frac{\nu\Sigma_4^{f}(\vec{r})}{\lambda}O_2^{+}(\vec{r})$$

$$-D_3(\vec{r})\nabla^2\phi_3^{+}(\vec{r})+\left[\Sigma_3^{A}(\vec{r})+\Sigma_3^{R}(\vec{r})\right]\phi_3^{+}(\vec{r}) = \chi_1\frac{\nu\Sigma_3^{f}(\vec{r})}{\lambda}\phi_1^{+}(\vec{r}) + \frac{\chi_2\,\nu\Sigma_3^{f}(\vec{r})}{\lambda}\phi_2^{+}(\vec{r})+\Sigma_3^{R}(\vec{r})\,\phi_4^{+}(\vec{r}) \qquad (24)$$

$$-D_2(\vec{r})\nabla^2\phi_2^+(\vec{r})+\left[\Sigma_2^A(\vec{r})+\Sigma_2^R(\vec{r})\right]\phi_2^+(\vec{r}) = \frac{\chi_1\,\nu\Sigma_2^f(\vec{r})\,\phi_1^+(\vec{r})}{\lambda} + \chi_2\frac{\nu\Sigma_2^f(\vec{r})\,\phi_2^+(\vec{r})}{\lambda}+\Sigma_2^R(\vec{r})\,\phi_3^+(\vec{r})$$

$$-D_1(\vec{r})\nabla^2\phi_1^+(\vec{r})+\left[\Sigma_1^A(\vec{r})+\Sigma_1^R(\vec{r})\right]\phi_1^+(\vec{r}) = \chi_1\frac{\nu\Sigma_1^f(\vec{r})\,\phi_1^+(\vec{r})}{\lambda} + \frac{\chi_2\,\nu\Sigma_1^f(\vec{r})\,\phi_2^+(\vec{r})}{\lambda}+\Sigma_1^R(\vec{r})\,\phi_2^+(\vec{r})$$

where the equations have been rearranged for convenience.

The manner in which to use the PDQ code in order to solve these equations is to alter, or "fool", the code by redefining the input quantities so that the above equations are solved in place of the regular diffusion equations. This redefinition of quantities for the PDQ calculation is shown in Table 18.

For a uniform core, i.e. only one fuel type, this redefinition would be exact. The 16 gram plate fuel regions were treated in this manner and are consistent with the definition of the χ values. These fuel regions are treated exactly. While it was possible to modify the thermal group cross section for the 18 gram plate regions so that the thermal group and the fast group were treated exactly, some error was incurred in these regions for the second and third groups. This is due to the coupling between groups where the same adjoint flux appears in two adjacent groups.

An estimate was made prior to the calculation to obtain the average energy in the second group. It appeared to be about 500 Kev so that it was felt that the input from the

TABLE 18

DEFINITION OF INPUT QUANTITIES FOR ADJOINT PDQ

Energy Group	D	Σ^A	Σ^R	Σ^f	χ_1	χ_2	χ_3
1	D_4	$\Sigma_4^A - \Sigma_3^R$	Σ_3^R	0	$C\ \chi_1$		
2	D_3	$\Sigma_3^A + \Sigma_3^R - \Sigma_2^R$	Σ_2^R	0		$\dfrac{C\ \chi_1 \nu \Sigma_3^f}{\nu \Sigma_4^f}$	
3	D_2	$\Sigma_2^A + \Sigma_2^R - \chi_2 \nu \Sigma_1^f - \Sigma_1^R$	$\chi_2 \nu \Sigma_1^f + \Sigma_1^R$	$\dfrac{\chi_2 \nu \Sigma_4^f}{\chi_1 \quad C}$			$\dfrac{C\ \chi_1 \nu \Sigma_2^f}{\nu \Sigma_4^f}$
4	D_1	$\Sigma_1^A + \Sigma_1^R - \chi_1 \nu \Sigma_1^f$	0	$\dfrac{\nu \Sigma_4^f}{C}$			

where $C = \dfrac{1}{\chi_1 + \dfrac{\chi_1 \nu \Sigma_3^f}{\nu \Sigma_4^f} + \dfrac{\chi_1 \nu \Sigma_2^f}{\nu \Sigma_4^f}}$

previous P-1 group independent buckling PDQ could be rearranged as input to the calculation. This was done and the calculation was performed. The input for the calculation is shown in Appendix H. The calculated core K_{eff} was 1.01059. An estimate of the error due to the assumptions regarding the 18 gram second and third energy group fission can be obtained by comparison with the core K_{eff} from the previously run corresponding PDQ. The error is only .01% Δ K, which is sufficiently good agreement to warrant saying that the adjoint fluxes obtained were fairly accurate.

Upon performing the laborious calculations needed to evaluate the effective delayed neutron fraction from Eqn. 23, a β(eff) of .0074 was obtained. This was in rather good agreement with the previously calculated value. However, when a check was made of the Group 2 average energy, this was found to be closer to 100 Kev than 500 Kev so that the result was suspect. For this additional reason, the earlier value of .0078 was taken for the analysis of experiments.

CHAPTER VI

COMPARISON OF ANALYTICAL MODEL WITH EXPERIMENT

A. Description of Reactor Experiments

A detailed description of the experiments will not be included. The data for the majority of the experiments for which calculations were done were obtained from Ref. 1. The remaining experiments were performed by the author during the course of the analysis.

Through necessity the experiments are separated in terms of the actual days on which the experiments were performed. This is done in an attempt to minimize the experimental error. Therefore to compare experiments performed on different days is to introduce uncertainties, such as the relation between console control rod dial positions and actual control rod positions. As has been shown by Dr. Fisher,[16] this type of error is minimal for experiments performed on the same day. Dr. Fisher quotes a value of $\pm 0.004\% \Delta \rho$ for measurements of the critical rod positions for the unperturbed core during a period of several hours on the same day with shims no. 1 and no. 2 brought to the same bank position and the regulating rod moved to attain criticallity in each measurement.

The types of experiments which were calculated involve the rearrangement of the core and reflector elements. There are several types of uncertainties that may be

incurred. These include change in control rod worth with core rearrangement, positioning of the elements in the core, and variation in fuel loading. An additional error is the type that involves the movement of one or both of the shim rods from one measurement to another. Therefore, when one or both of the shim rods are moved, there is some error in obtaining the change in reactivity relative to a base condition. This is due to the way in which the calibration curves for the shim rods were obtained. The calibration curve for shim no. 1 was obtained by rod interchange with the regulating rod over the major portion of the curve. However shim no. 2 was employed in a portion of the calibration, with the consequence that some interaction effects were included. Similarly for the calibration of shim no. 2 there were interaction effects due to the use of shim no. 1. Consequently when shim no. 1 or both shims are moved in an experiment, and the reactivity worth relative to a base configuration with the different shim positions is desired, then some error is incurred due to these effects.

Dr. Fisher has made an estimate of the reactivity uncertainty associated with the positioning of a sample holder in the core to be $\pm 0.01\% \Delta\rho$ which can be assumed to be the reactivity uncertainty associated with the positioning of an element in the core when the control rod shim positions are kept constant. In cases where the shim positions differ from those for the condition from which the reactivity difference is desired, the error

may be somewhat larger.

The uncertainty due to variation in fuel loading can be roughly estimated by utilizing data from Ref. 1 that was obtained in the addition of the "outer glory hole" fuel plates in the semi-permanent core configuration. The change in reactivity that was obtained with the addition of the 4 fuel plates, containing 18 grams of U-235 per plate, was $+0.44\%\Delta\rho$. This corresponds to a fuel coefficient of $+0.006\%\Delta\rho$ per gram of U-235. This does not account for the variation in flux level with core position but should be a reasonable estimate of the average core fuel coefficient. Since the majority of the experiments involve the movement of the "inner glory hole" and a fuel element containing 10 fuel plates with 16 grams of U-235 per plate, the uncertainty due to variation in fuel loading should be approximately $\pm 0.02\%\Delta\rho$. The total error then, neglecting the change in control rod worth with core rearrangement and the movement of the shim rods relative to the base configuration, is taken to be approximately $\pm 0.02\%\Delta\rho$.

The experimental configurations, for which calculations were done, are described in Table 19 grouped by the days on which the experiments were performed. The first configuration in each time period is taken to be the base case and reactivity differences are shown relative to this experiment for initial analysis. The corrected reactivity values shown are obtained using the control

TABLE 19

EXPERIMENTAL CONFIGURATIONS

Exp. no.	Date	No. of Fuel Plates and Comments	I.G.H. Facing Side	I.G.H. Location in Core	Shim no. 1 cm	Shim no. 2 cm	Reg. Rod cm	Exp. ρ(%)	Exp. $\Delta\rho$(%)
1	3/20/62	162	West	D-6	out	out	40.85	0.081	
2	"	162	East	C-5	36.38	out	in	0.968	+0.888
3	"	162	East	D-5	47.69	out	out	0.165	+0.084
4	"	162	North	D-5	46.75	out	18.75	0.485	+0.404
5	"	162	North	D-6	46.73	out	in	0.566	+0.485
6	"	162	East	D-6	46.74	out	21.81	0.453	+0.372
7	"	162	East	E-5	54.56	out	out	0.031	-0.050
8	4/2/62	162	East	D-5	47.69	out	out	0.165	
9	"	162	North	D-5	out	out	26.31	0.212	+0.047
10	4/16/62	166 with O.G.H. facing North in B-5	North	D-5	46.02	45.96	33.80	0.726	
11	"	166 with O.G.H. facing West in B-5	North	D-5	46.00	46.00	52.30	0.603	-0.123

Table 19, Cont'd

Exp. no.	Date	No. of Fuel Plates and Comments	I.G.H. Facing Side	I.G.H Location in Core	Shim no. 1 cm	Shim no. 2 cm	Reg. Rod cm	Exp. ρ(%)	Exp. $\Delta\rho$(%)
12	11/10/67	166 with O.G.H. facing North in B-5	North	D-5	44.00	out	16.62	0.579	
13	"	166 with O.G.H. facing South in B-5	North	D-5	44.00	out	48.10	0.313	-0.266
14	"	166 with O.G.H. facing South in B-4	North	D-5	44.00	out	46.99	0.318	-0.261

rod calibration curves given in Ref. 1 and correcting the resulting reactivity difference by the ratio of the effective delayed neutron fraction to the infinite core value, i.e. by about 3%.

The terminology O.G.H. and I.G.H. is used to designate the "outer glory hole" and "inner glory hole" fuel elements respectively. The experiments with 162 fuel plates in the core are similar in the respect that location F-3 contained 10 fuel plates, with 18 grams of U-235 per plate, while the element in F-8 contained 10 fuel plates with 16 grams of U-235 per plate. In the experiments with 166 fuel plates these two elements were reversed. A typical configuration with 162 fuel plates, i.e. that for Exp. no. 1, is shown in Fig. 2.

When the terminology that O.G.H. or I.G.H. is facing side X is used, it is meant that the "glory hole" element is so located that the water, i.e. that portion of the element with the fuel plates removed, fills the X quadrant of the element location.

A graphite element is located in B-5 in all the experiments in which the core is loaded with 162 fuel plates, with the exception of Exp. no. 9 where the graphite element has been replaced with water.

The core configurations are the same as the semi-permanant arrangement shown in Fig. 1 for all the experiments in which the core was loaded with 166 fuel plates, with the exceptions as noted in Table 19, i.e. the "outer glory hole" was moved from one core location to another or oriented in a different manner.

B. Calculations for Experiments

PDQ calculations were performed for the experiments listed in Table 19 to determine the ability of the calculational model to predict reactivity changes. The calculations were done with the fast group cross sections obtained using a GAM energy independent buckling and Wigner-Wilkins thermal cross sections as previously discussed. An iterative procedure was not used since it was shown earlier that the calculated K_{eff} was not extremely sensitive to small changes in the GAM buckling. Thus the cross sections were taken to be the same as for the semi-permanent core result listed in Table 11, for the P-1 energy independent case, and shown in Fig. 4. The results of the calculations are given by the corresponding experiment number from Table 19 in Table 20. The experimental $\Delta\rho$'s for the change in reactivity from the base case are reproduced from Table 18 for comparison with the calculated $\Delta\rho$'s for the initial comparison.

TABLE 20

RESULTS OF CALCULATIONS OF EXPERIMENTS

Exp no.	Date	Calc. K_{eff}	Calc. ρ (%)	Calc. $\Delta\rho$ (%)	Exp. $\Delta\rho$ (%)	Exp. $\Delta\rho$ - Calc. $\Delta\rho$ (%)
1	3/20/62	1.00275	0.274			
2	"	1.01082	1.070	+0.796	+0.888	+0.092
3	"	1.00341	0.340	+0.066	+0.084	+0.019
4	"	1.00644	0.640	+0.366	+0.404	+0.038
5	"	1.00694	0.689	+0.415	+0.485	+0.070
6	"	1.00622	0.618	+0.342	+0.372	+0.030
7	"	1.00142	0.142	-0.132	-0.050	+0.082

Table 20, Cont'd

Exp. no.	Date	Calc. K_{eff}	Calc. ρ(%)	Calc. $\Delta\rho$(%)	Exp. $\Delta\rho$(%)	Exp.$\Delta\rho$-Calc.$\Delta\rho$ (%)
8	4/2/62	1.00341	0.340			
9	"	1.00361	0.360	+0.020	+0.047	+0.027
10	4/16/62	1.01048	1.037			
11	"	1.00948	0.939	-0.098	-0.123	-0.025
12	11/10/67	1.01048	1.037			
13	"	1.00787	0.781	-0.256	-0.266	-0.010
14	"	1.00780	0.774	-0.263	-0.261	+0.002

The calculated $\Delta\rho$'s are in fairly good agreement with the experimental values. The largest variation that would have occurred if the calculated reactivity changes had been used to predict an experimental reactivity would have been -0.092%$\Delta\rho$. The mean, or average, in terms of the absolute values of the differences between the calculated and experimental reactivity changes is only 0.04%, while the mean of the absolute values of the experimental reactivity changes is 0.298%$\Delta\rho$. This would amount to a difference between predicted and experimental reactivities of 0.04%$\Delta\rho$ on the average.

While the difference between predicted and experimental reactivities on an average basis is acceptable for most practical purposes, considerable improvement can be obtained if an attempt is made to eliminate some of the experimental uncertainties. These include, as described previously, the uncertainty that is introduced when measurements utilizing different shim positions are compared and also the change in rod worth with core configuration. To eliminate the first of these uncertainties

the experiments and calculations are compared for those conditions where the shim positions remain almost constant relative to a base configuration. This comparison is shown in Table 21.

TABLE 21

COMPARISON OF CALCULATIONS AND EXPERIMENTS FOR APPROXIMATELY CONSTANT SHIM POSITIONS

Exp. no.	Date	Calc. ρ(%)	Calc. $\Delta\rho$(%)	Exp. $\Delta\rho$(%)	Exp.$\Delta\rho$ - Calc.$\Delta\rho$ (%)
3	3/20/62	0.340			
4	"	0.640	+0.300	+0.320	+0.020
5	"	0.689	+0.349	+0.401	+0.052
6	"	0.618	+0.278	+0.288	+0.010
10	4/16/62	1.037			
11	"	0.939	-0.098	-0.123	-0.025
12	11/10/67	1.037			
13	"	0.781	-0.256	-0.266	-0.010
14	"	0.774	-0.263	-0.261	+0.002

The results in Table 21 show that the maximum error that would be experienced if calculational results were used to predict experimental reactivity changes would be -0.052%$\Delta\rho$. The average or mean of the absolute value of the experimental reactivity change is 0.277%$\Delta\rho$ while the mean of the absolute difference between calculated and experimental reactivity changes is 0.02%. This would mean an error of 0.02% in $\Delta\rho$ on the average if the calculated results had been used to predict experimental reactivity changes. It should be observed that improvement was obtained in the mean difference between calculated and experimental reactivity changes

by considering only those experiments where the shim positions remain approximately constant. In addition, the mean difference is only on the order of the experimental uncertainty, neglecting the change in control rod worth with core configuration.

While the agreement between calculational and experimental results is quite good, especially for the special case where the shim positions remain approximately constant, it is evident from the data in Tables 20 and 21 that the calculations consistently underestimate the change in reactivity compared to experiment. This is felt to be partially due to the calculational model rather than such possibilities as the effective delayed neutron fraction or uncertainties in the control rod calibration curves. One such likely factor with regard to the calculational model, is the overestimate of the thermal diffusion lengths as predicted using the Wigner-Wilkins model. This should tend to underestimate the reactivity worth of the water in the glory hole element. It is recommended for future work that the use of Maxwellian thermal diffusion coefficients with Wigner-Wilkins thermal cross sections be investigated.

CHAPTER VII

CONCLUSIONS AND RECOMMENDATIONS

Several cross section models, which were used with a two-dimensional group diffusion method, were compared with experiment for the semi-permanent core configuration. All of these cross section models, with the exception of that using thermal group cross sections averaged over an unhardened Maxwell-Boltzmann thermal spectrum, were found to give reasonable agreement with the experimental value of the excess reactivity for the semi-permanent core configuration. These models are attractive in that they tend to minimize errors that may occur with cruder methods, such as hand calculations, while utilizing less computer time than more sophisticated models, for example, such as a three-dimensional diffusion theory technique or a two-dimensional Sn type method with an equivalent number of mesh points.

The method using fast group cross sections obtained by using the volume integrated P-1 equations in the GAM code with an energy independent buckling, and thermal group cross sections using the Wigner-Wilkins thermal spectrum model, gave the closest agreement with the experimental value of the excess reactivity for the semi-permanent core configuration. The difference between the calculated reactivity, using this cross section model with the two-dimensional group diffusion technique, and the experimental value of the excess reactivity was only 0.02% $\Delta\rho$.

This agreement was fortuitous, and was certainly the result of cancellation of errors. In addition, the cross section model using fast group cross sections obtained from the B-1 method should, theoretically, give the closest agreement with experiment. However the difference between the calculated core reactivity and the experimental value was only 0.3%$\Delta\rho$ using the B-1 method, which was still in good agreement when the uncertainties of the calculations were considered.

The cross section model using fast group cross sections obtained utilizing the P-1 equations with an energy independent buckling, and thermal group cross sections obtained with the Wigner-Wilkins thermal spectrum model, was chosen for the analysis of the experiments. This choice was made solely on the basis that this model agreed closest with experiment for the semi-permanent core configuration. The agreement between calculated reactivity changes and experimental reactivity changes, obtained with core rearrangement, was good. The closest agreement, between calculated and experimental reactivity changes, was shown for those particular cases when the shim rod positions were kept approximately constant in going from one experimental configuration to another. It is felt that the agreement between calculations and experiment is such that the calculational model could be used to predict reactivity changes that would occur with core rearrangement, to within reasonable limits of accuracy.

It does appear, however, that the calculational model slightly underpredicts reactivity changes when compared with experiment. This is felt to be due to the calculational model, rather than to such factors as uncertainty in the experimental results or the value of the delayed neutron fraction that was used in the analysis of the experiments. In particular, the Wigner-Wilkins thermal spectrum model classically overestimates thermal diffusion lengths. This would tend to underestimate the reactivity worth of the water in the "glory hole" regions, with the result that the calculational model would tend to underestimate reactivity changes with core rearrangement for the experiments that were considered. It is recommended that the use of Maxwell-Boltzmann thermal diffusion coefficients, with Wigner-Wilkins thermal group cross sections, be investigated in future analysis. This should enhance the flux gradients in the "glory hole" water regions, thereby increasing the reactivity worth of these regions.

It is also recommended that the second method, i.e. that in which an adjoint or weighting function is used to determine the relative importance of delayed neutrons, be investigated further. It should be apparent that for any investigation of reactor experiments, an accurate value of the delayed neutron fraction is needed. While the value used in this analysis appears to be reasonable, it is important that as accurate a value as possible be obtained.

APPENDIX A

CORE AND REFLECTOR CROSS SECTIONS FOR R-Z PDQ

Group	Composition	D cm	Σ^A cm^{-1}	Σ^R cm^{-1}	$\nu\Sigma^f$ cm^{-1}
1	1	2.07109	0.000602	0.105473	0.0
1	2	2.176673	0.000445	0.081039	0.0
1	3	2.294562	0.000299	0.057285	0.0
1	4	2.340347	0.000079	0.037970	0.0
1	5	2.134925	0.000531	0.084899	0.000371
2	1	1.067550	0.0	0.147215	0.0
2	2	1.152311	0.000146	0.102864	0.0
2	3	1.283861	0.000277	0.061859	0.0
2	4	1.478003	0.000056	0.037685	0.0
2	5	1.307966	0.000347	0.103461	0.000461
3	1	0.607451	0.000800	0.150213	0.0
3	2	0.807761	0.000753	0.104359	0.0
3	3	1.184133	0.000708	0.061876	0.0
3	4	1.111625	0.000197	0.030317	0.0
3	5	0.999543	0.005369	0.103078	0.006750
4	1	0.15970	0.01923		0.0
4	2	0.22740	0.01711		0.0
4	3	0.37390	0.01505		0.0
4	4	0.943174	0.004616		0.0
4	5	0.503736	0.058489		0.088466

APPENDIX B

PDQ ABOVE THERMAL GROUP CONSTANTS FOR P-1 VARIABLE B^2

Energy Group	Composition	D cm	Σ^A cm^{-1}	Σ^R cm^{-1}	$\nu\Sigma^f$ cm^{-1}
1	8	1.962643	0.000462	0.112631	0.0
1	9	2.743129	0.000246	0.014369	0.0
1	10	2.115374	0.000406	0.087080	0.0
1	11	2.138534	0.000635	0.082931	0.000673
1	12	2.139309	0.000609	0.082910	0.000598
1	13	2.208013	0.000376	0.073448	0.0
1	14	2.256550	0.000361	0.066795	0.0
1	15	2.145523	0.000397	0.082742	0.0
2	8	1.166225	0.0	0.144057	0.0
2	9	2.222087	0.000471	0.000805	0.0
2	10	1.225451	0.000122	0.106807	0.0
2	11	1.237008	0.000535	0.100481	0.000846
2	12	1.237707	0.000492	0.100481	0.000752
2	13	1.277776	0.000188	0.086934	0.0
2	14	1.310102	0.000220	0.077234	0.0
2	15	1.240329	0.000143	0.100483	0.0
3	8	0.638765	0.000769	0.143780	0.0
3	9	3.931000	0.000630	0.000634	0.0
3	10	0.816226	0.000733	0.106558	0.0
3	11	0.836311	0.009406	0.100236	0.012625
3	12	0.838495	0.008444	0.100237	0.011222
3	13	0.958303	0.000713	0.086699	0.0
3	14	1.047300	0.000704	0.077006	0.0
3	15	1.856648	0.000727	0.100237	0.0

APPENDIX C

PDQ ABOVE THERMAL GROUP CONSTANTS FOR B-1 GAM $B^2 = 0.0112\ cm^{-2}$

Energy Group	Composition	D cm	Σ^A cm^{-1}	Σ^R cm^{-1}	$\nu\Sigma^f$ cm^{-1}
1	8	1.763362	0.000482	0.111821	0.0
1	9	2.480532	0.000258	0.014325	0.0
1	10	1.902365	0.000423	0.086469	0.0
1	11	1.927729	0.000652	0.082354	0.000674
1	12	1.928428	0.000626	0.082333	0.000599
1	13	1.986959	0.000392	0.072944	0.0
1	14	2.031371	0.000377	0.066342	0.0
1	15	1.928428	0.000413	0.082165	0.0
2	8	1.025415	0.0	0.142956	0.0
2	9	2.195342	0.000468	0.000797	0.0
2	10	1.108025	0.000122	0.105990	0.0
2	11	1.125730	0.000534	0.099712	0.000844
2	12	1.126366	0.000490	0.099712	0.000750
2	13	1.172097	0.000187	0.086268	0.0
2	14	1.210619	0.000218	0.076642	0.0
2	15	1.126366	0.000142	0.099713	0.0
3	8	0.605128	0.000756	0.141290	0.0
3	9	3.921372	0.000624	0.000621	0.0
3	10	0.775905	0.000722	0.104712	0.0
3	11	0.795416	0.009347	0.098500	0.012551
3	12	0.797496	0.008390	0.098500	0.011157
3	13	0.912941	0.000704	0.085197	0.0
3	14	0.999257	0.000695	0.075672	0.0
3	15	0.797496	0.000716	0.098501	0.0

APPENDIX D

THERMAL GROUP MAXWELLIAN CROSS SECTIONS FOR PDQ

Energy Group	Composition	D cm	Σ^A cm^{-1}	$\nu\Sigma^f$ cm^{-1}
4	1	0.153500	0.019660	0.0
4	2	0.915000	0.000266	0.0
4	3	3.492500	0.012925	0.0
4	4	0.153500	0.019660	0.0
4	5	3.492500	0.012925	0.0
4	6	0.281600	0.010660	0.0
4	7	0.905000	0.000266	0.0
4	8	0.153500	0.019660	0.0
4	9	3.492500	0.012925	0.0
4	10	0.204000	0.017910	0.0
4	11	0.202900	0.123000	0.218200
4	12	0.204100	0.111300	0.193900
4	13	0.247400	0.016980	0.0
4	14	0.276200	0.016520	0.0
4	15	0.216100	0.017610	0.0

APPENDIX E

PDQ ABOVE THERMAL GROUP CONSTANTS FOR P-1 GAM $B^2 = 0.005$ cm^{-2}

Energy Group	Composition	D cm	Σ^A cm^{-1}	Σ^R cm^{-1}	$\nu\Sigma^f$ cm^{-1}
1	8	1.985519	0.000496	0.111124	0.0
1	9	2.754126	0.000266	0.014281	0.0
1	10	2.136829	0.000436	0.085942	0.0
1	11	2.158013	0.000665	0.081856	0.000675
1	12	2.158795	0.000638	0.081834	0.000600
1	13	2.228124	0.000404	0.072507	0.0
1	14	2.277103	0.000389	0.065949	0.0
1	15	2.165065	0.000426	0.081666	0.0
2	8	1.060106	0.0	0.145909	0.0
2	9	2.232018	0.000475	0.000819	0.0
2	10	1.140488	0.000123	0.108181	0.0
2	11	1.151382	0.000538	0.101773	0.000849
2	12	1.152032	0.000495	0.101773	0.000755
2	13	1.202094	0.000189	0.088053	0.0
2	14	1.222850	0.000221	0.078228	0.0
2	15	1.157724	0.000144	0.101775	0.0
3	8	0.605761	0.000773	0.144796	0.0
3	9	3.934720	0.000633	0.000640	0.0
3	10	0.776573	0.000737	0.107311	0.0
3	11	0.796287	0.009431	0.100946	0.012656
3	12	0.798367	0.008467	0.100946	0.011249
3	13	0.913721	0.000717	0.087313	0.0
3	14	0.997148	0.000708	0.077551	0.0
3	15	0.815625	0.000731	0.100947	0.0

APPENDIX F

PDQ ABOVE THERMAL GROUP CONSTANTS FOR P-1 GAM B^2 = .014 cm^{-2}

Energy Group	Composition	D cm	Σ^A cm^{-1}	Σ^R cm^{-1}	$\nu\Sigma^f$ cm^{-1}
1	8	1.962643	0.000462	0.112631	0.0
1	9	2.743129	0.000246	0.014369	0.0
1	10	2.115347	0.000406	0.087080	0.0
1	11	2.138534	0.000635	0.082931	0.000673
1	12	2.139309	0.000609	0.082910	0.000598
1	13	2.208013	0.000376	0.073448	0.0
1	14	2.256550	0.000361	0.066795	0.0
1	15	2.145523	0.000397	0.082742	0.0
2	8	1.068620	0.0	0.142872	0.0
2	9	2.219102	0.000468	0.000796	0.0
2	10	1.146872	0.000122	0.105928	0.0
2	11	1.158619	0.000534	0.099653	0.000844
2	12	1.159274	0.000490	0.099653	0.000750
2	13	1.209650	0.000187	0.086218	0.0
2	14	1.247359	0.000218	0.076598	0.0
2	15	1.165002	0.000142	0.099655	0.0
3	8	0.610940	0.000756	0.141246	0.0
3	9	3.915276	0.000624	0.000621	0.0
3	10	0.782665	0.000722	0.104679	0.0
3	11	0.802410	0.009346	0.098469	0.012550
3	12	0.804505	0.008389	0.098469	0.011156
3	13	0.920746	0.000704	0.085170	0.0
3	14	1.007505	0.000695	0.075648	0.0
3	15	0.821896	0.000716	0.098470	0.0

APPENDIX G

PDG ABOVE THERMAL GROUP CONSTANTS FOR B-1 GAM $B^2 = 0.005$ cm^{-2}

Energy Group	Composition	D cm	Σ^A cm^{-1}	Σ^R cm^{-1}	$\nu\Sigma^f$ cm^{-1}
1	8	1.898206	0.000501	0.110956	0.0
1	9	2.643816	0.000269	0.014273	0.0
1	10	2.044830	0.000440	0.085815	0.0
1	11	2.066596	0.000669	0.081736	0.000675
1	12	2.067345	0.000642	0.081715	0.000600
1	13	2.136280	0.000408	0.072403	0.0
1	14	2.180642	0.000392	0.065856	0.0
1	15	2.073350	0.000430	0.081547	0.0
2	8	1.043645	0.0	0.145921	0.0
2	9	2.223304	0.000475	0.000819	0.0
2	10	1.124396	0.000123	0.108190	0.0
2	11	1.136659	0.000538	0.101782	0.000849
2	12	1.137301	0.000495	0.101782	0.000755
2	13	1.189323	0.000189	0.088060	0.0
2	14	1.223717	0.000221	0.078235	0.0
2	15	1.142921	0.000144	0.101783	0.0
3	8	0.606056	0.000773	0.144802	0.0
3	9	3.930225	0.000633	0.000640	0.0
3	10	0.774049	0.000737	0.107316	0.0
3	11	0.793724	0.009431	0.100950	0.012656
3	12	0.795797	0.008467	0.100950	0.011250
3	13	0.930689	0.000717	0.087316	0.0
3	14	1.018683	0.000708	0.077554	0.0
3	15	0.813000	0.000731	0.100951	0.0

APPENDIX H

CORE AND REFLECTOR CROSS SECTIONS FOR ADJOINT PDQ

Energy Group	Composition	D cm	Σ^A cm^{-1}	Σ^R cm^{-1}	$\nu\Sigma^f$ cm^{-1}
1	1	0.159700	-0.130983	0.150213	0.0
1	2	0.915000	-0.006362	0.006626	0.0
1	3	4.039510	0.011952	0.000628	0.0
1	4	0.159700	-0.131663	0.150893	0.0
1	5	3.518041	0.011909	0.000677	0.0
1	6	0.291141	-0.061966	0.072350	0.0
1	7	0.914610	-0.006120	0.006381	0.0
1	8	0.159700	-0.123102	0.142332	0.0
1	9	4.039510	0.011953	0.000626	0.0
1	10	0.213900	-0.088054	0.105484	0.0
1	11	0.261000	0.003373	0.099227	0.0
1	12	0.258100	-0.004977	0.099227	0.0
1	13	0.261000	-0.069376	0.085826	0.0
1	14	0.294200	-0.060270	0.076230	0.0
1	15	0.226900	-0.082108	0.099228	0.0
2	1	0.607451	0.003798	0.147215	0.0
2	2	0.933637	-0.004281	0.010907	0.0
2	3	3.844500	0.000451	0.000804	0.0
2	4	0.593056	-0.009350	0.161046	0.0
2	5	3.982634	0.000412	0.000914	0.0
2	6	0.793107	-0.004653	0.077448	0.0
2	7	0.933149	-0.000920	0.007301	0.0
2	8	0.609331	-0.000704	0.143798	0.0
2	9	3.934169	0.000450	0.000803	0.0
2	10	0.780906	-0.000404	0.106615	0.0
2	11	0.800677	0.008299	0.100299	0.0
2	12	0.802768	0.007340	0.100300	0.0
2	13	0.918758	-0.000244	0.086777	0.0
2	14	1.005330	-0.000165	0.077095	0.0
2	15	0.820122	-0.000353	0.100301	0.0
3	1	1.067550	0.041742	0.105473	0.0
3	2	1.081446	-0.013449	0.024356	0.0
3	3	2.224563	-0.013129	0.014402	0.0
3	4	0.966714	0.035875	0.125171	0.0
3	5	2.287087	-0.013874	0.015307	0.0
3	6	1.628830	0.009325	0.068182	0.0
3	7	1.122183	-0.013251	0.020552	0.0
3	8	1.065928	0.031574	0.112223	0.0
3	9	2.223044	-0.013071	0.014344	0.0
3	10	1.144522	0.019965	0.086772	0.0
3	11	1.156339	0.018028	0.082806	0.047958
3	12	1.156993	0.018025	0.082766	0.043252

Appendix H, Cont'd

Energy Group	Composition	D cm	Σ^A cm^{-1}	Σ^R cm^{-1}	$\nu\Sigma^f$ cm^{-1}
3	13	1.207270	0.013772	0.073193	0.0
3	14	1.244905	0.010748	0.066565	0.0
3	15	1.162710	0.017994	0.082450	0.0
4	1	2.071090	0.106075		0.0
4	2	2.377797	0.024356		0.0
4	3	2.739952	0.014645		0.0
4	4	1.834713	0.125527		0.0
4	5	2.675552	0.015496		0.0
4	6	2.124839	0.068368		0.0
4	7	2.426979	0.020552		0.0
4	8	1.968672	0.112694		0.0
4	9	2.746000	0.014595		0.0
4	10	2.114435	0.087186		0.0
4	11	2.142498	0.082776		0.146677
4	12	2.143274	0.082784		0.132284
4	13	2.212105	0.073576		0.0
4	14	2.260732	0.066934		0.0
4	15	2.149500	0.082854		0.0

SELECTED BIBLIOGRAPHY

1. A. Diaz, J. Fisher, "Criticality Experiments with the University of Maryland Reactor," Nuclear Engineering, University of Maryland, Oct. 30, 1962

2. D. Duffey, et al., "Safeguards Evaluation of the University of Maryland Reactor," February 7, 1960

3. G. G. Bilodeau, et al., "PDQ, An IBM-704 Code to Solve the Two-Dimensional Few Group Diffusion Equations," WAPD-TM-70 (August 1957)

4. O. J. Marlowe, E. M. Gelbard, "WANDA - A One-Dimensional Few-Group Diffusion Equation Code for the IBM-704," WAPD-TM-28, November, 1956

5. D. J. Hughes, R. B. Schwartz, "Neutron Cross Sections," BNL-325, Second Edition, 1958

6. J. S. Dudek, G. D. Joanou, "GAM-1: A Consistent P-1 Multigroup Code for the Calculation of Fast Neutron Spectra and Multigroup Constants," GA-1850, June 28, 1961

7. A. M. Weinberg, E. P. Wigner, "The Physical Theory of Neutron Chain Reactors," University of Chicago Press, 1958

8. G. C. Pomraning, "On the Energy Averaging of the Diffusion Coefficients," Nuclear Science and Engineering, Vol. 19, No. 2, June 1964

9. S. Glasstone, M. Edlund, "The Elements of Nuclear Reactor Theory," D. Van Nostrand Co., Inc., 1960

10. E. P. Wigner, J. E. Wilkins, "Effect of the Temperature of the Moderator on the Velocity Distribution of Neutrons with Numerical Calculations for H as Moderator," AECD-2275, September 14, 1944

11. R. H. Shuddle, J. Dyer, "TEMPEST II, A Neutron Thermalization Code," AMTD-111, June 1962

12. B. Davison, "Neutron Transport Theory," Oxford University Press, 1958

13. R. L. Murray, "Nuclear Reactor Physics," Prentice-Hall, Inc., 1957

14. Argonne National Laboratory, "Reactor Physics Constants," ANL-5800, Second Edition, July 1963

15. A. Radkowsky, Editor, "Naval Reactors Physics Handbook," Vol. 1, 1964

16. J. Fisher, "The Utilization and Effectiveness of Linear Arrays of Neutron Absorber Filled Tubes as Control Rods in Water Moderated Nuclear Reactors," Ph.D. Thesis, University of Maryland (1964)

17. R. S. Marsden, et al., "Reactor Physics Studies for the Final Conceptual Design of the Advanced Test Reactor," IDO-16668, March 24, 1961

18. C. H. Westcott, et al., "Survey of Nuclear Data for Reactor Calculations," Proceedings of the Third International Conference, Vol. 2, Geneva, 1964

19. H. Etherington, "Nuclear Engineering Handbook," McGraw-Hill, 1958

20. R. Perez-Belles, et al., "A Measurement of the Effective Delayed Neutron Fraction for the BSR-1," Nuclear Science and Engineering, Vil. 12, No. 4, April, 1962

21. W. R. Cadwell, "PDQ-5 - A FORTRAN Program for the Solution of the Two-Dimensional Neutron-Diffusion Problem - Part I: Steady-State Version," WAPD-TM-363, February, 1963

22. A. F. Henry, "The Application of Reactor Kinetics to the Analysis of Experiments," Nuclear Science and Engineering, Vol. 3, No. 1, January, 1958

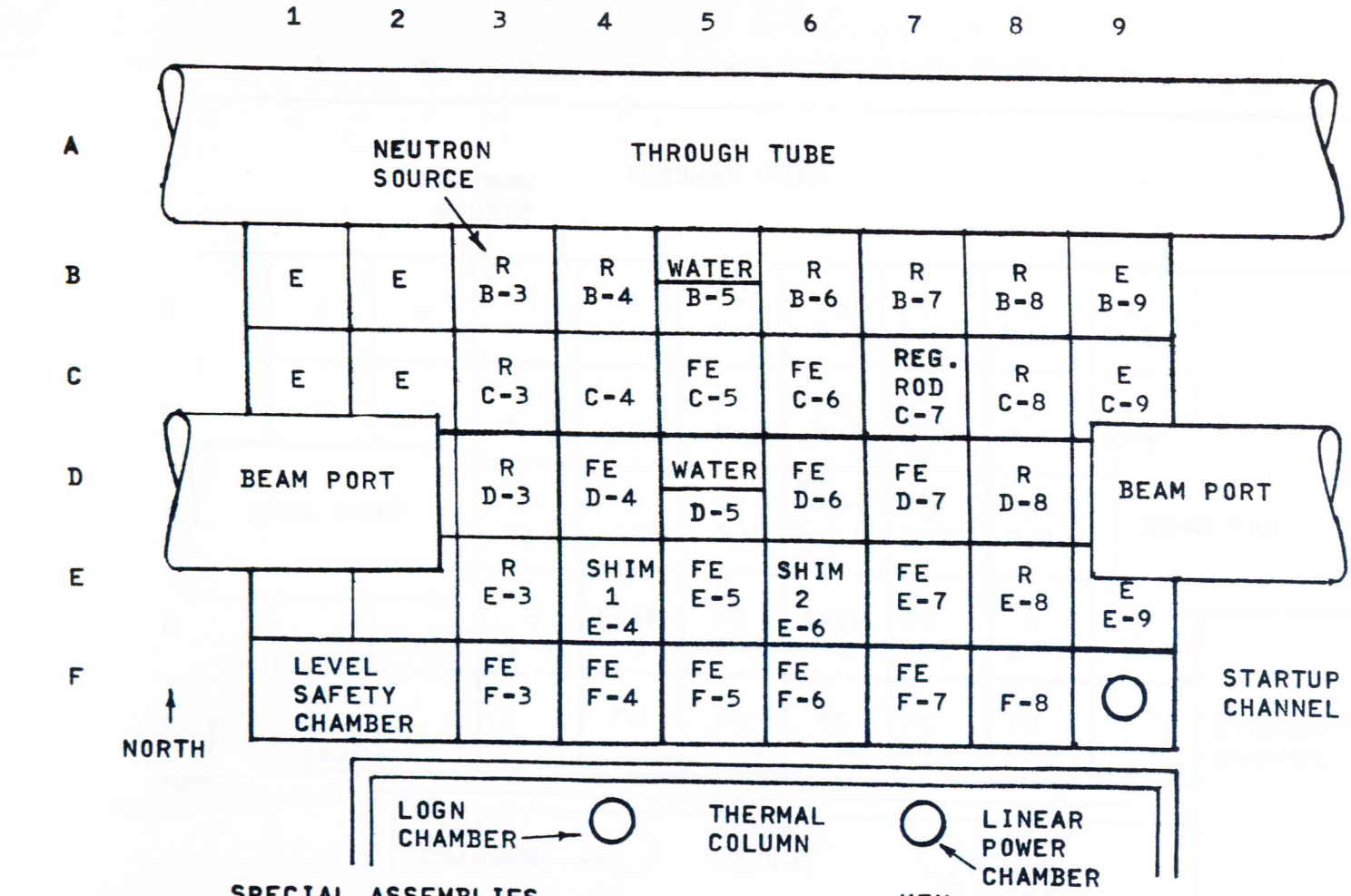

SPECIAL ASSEMBLIES

F-8 TEN 18 GM U-235 FUEL PLATES

E-4, C-7, E-6 SIX 16 GM U-235 FUEL PLATES

B-5 FOUR 18 GM U-235 FUEL PLATES + ONE AL PLATE

C-4 NINE 16 GM U-235 FUEL PLATES + ONE AL PLATE

D-5 FIVE 18 GM U-235 FUEL PLATES + ONE AL PLATE

KEY

E - EMPTY GRID POSITION

R - GRAPHITE REFLECTOR ASSEMBLY

FE- FUEL ASSEMBLY LOADED WITH 10 16 GM U-235 FUEL PLATES

FIG. 1

SEMI-PERMANENT CORE CONFIGURATION

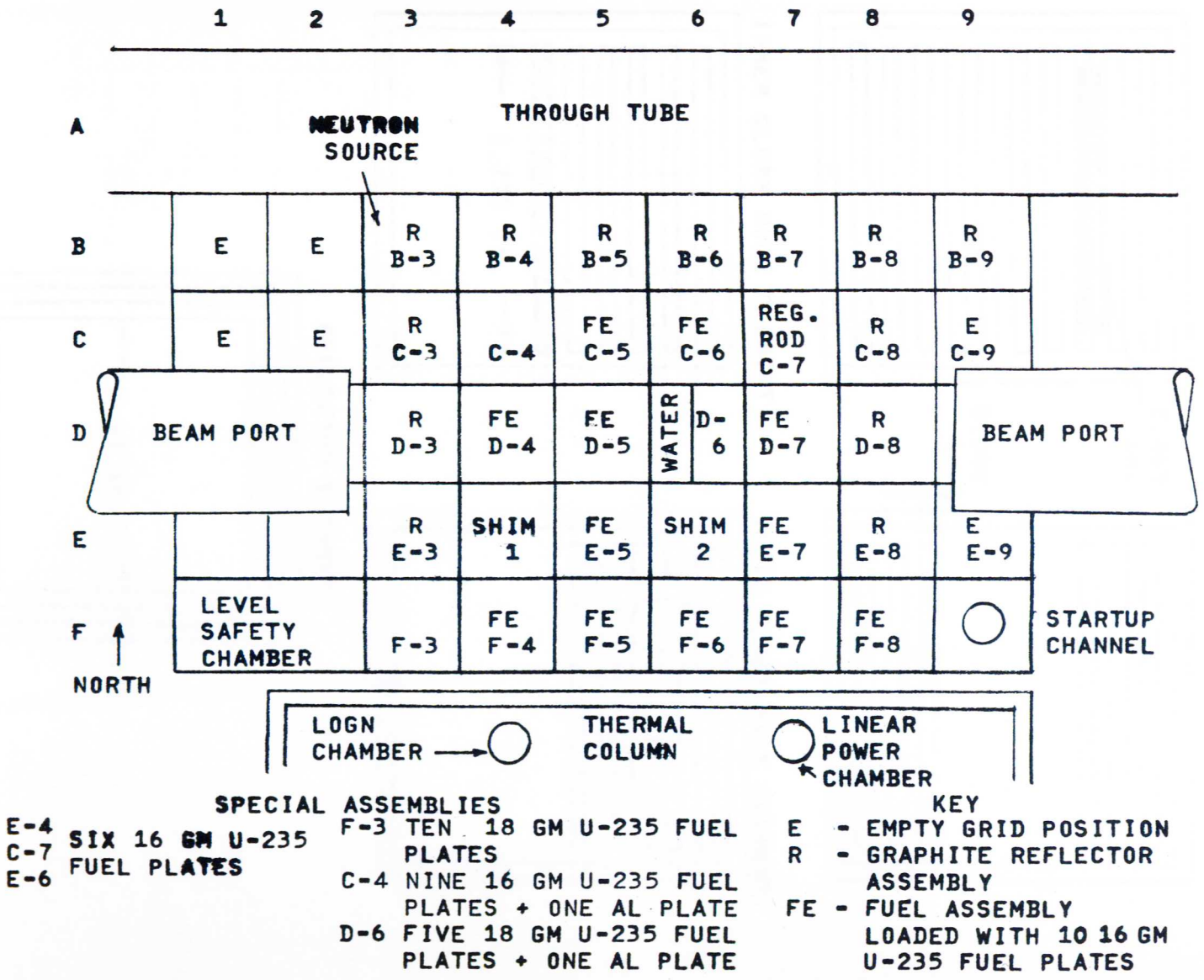

FIG. 2

CORE CONFIGURATION FOR EXPERIMENT NO. 1

FIG. 3

CORE AND REFLECTOR ASSEMBLIES

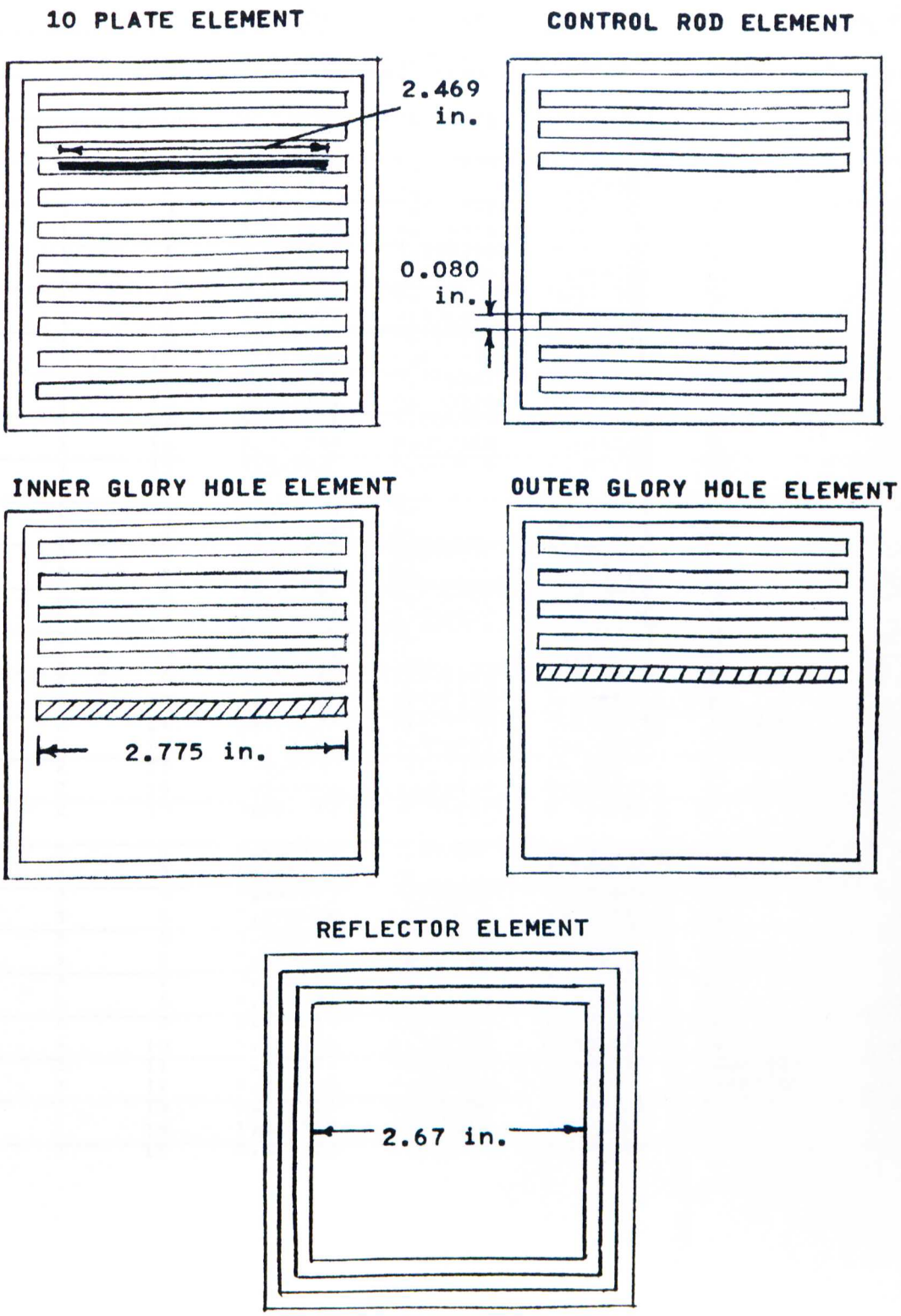

FIG.4

UOFM FULL CORE CALCULATION 166 PLATES XY PDQ02

4 GROUPS 15 COMPS SS= 68 TT= 76 B.C.=0,0,0,0

B SQ	LAMBDA	EPSILON	CHI 1	CHI 2	CHI 3
0.001600	1.010000	0.020000	0.753600	0.246400	0.

GROUP	COMP	D	SIGMA A	SIGMA R	NU SIGMA F	PHI
1	1	2.071090	0.000602	0.105473	0.	2.000
1	2	2.377797	0.	0.024356	0.	1.950
1	3	2.739952	0.000242	0.014402	0.	42.000
1	4	1.834713	0.000356	0.125171	0.	31.400
1	5	2.675552	0.000189	0.015307	0.	31.500
1	6	2.124839	0.000186	0.068182	0.	31.200
1	7	2.426979	0.	0.020552	0.	30.700
1	8	1.968672	0.000471	0.112223	0.	100.000
1	9	2.746000	0.000251	0.014344	0.	100.000
1	10	2.114435	0.000414	0.086772	0.	100.000
1	11	2.142498	0.000643	0.082640	0.000673	100.000
1	12	2.143274	0.000616	0.082619	0.000598	100.000
1	13	2.212105	0.000383	0.073193	0.	100.000
1	14	2.260732	0.000368	0.066565	0.	100.000
1	15	2.149500	0.000404	0.082450	0.	100.000
2	1	1.067550	0.	0.147215	0.	4.000
2	2	1.081446	0.	0.010907	0.	5.200
2	3	2.224563	0.000470	0.000804	0.	61.600
2	4	0.966714	0.	0.161046	0.	41.900
2	5	2.287087	0.000519	0.000914	0.	42.100
2	6	1.028830	0.000060	0.077448	0.	42.200
2	7	1.122183	0.	0.007301	0.	42.800
2	8	1.065928	0.	0.143798	0.	100.000
2	9	2.223044	0.000470	0.000803	0.	100.000
2	10	1.144522	0.000122	0.106615	0.	100.000
2	11	1.156339	0.000535	0.100299	0.000844	100.000
2	12	1.156993	0.000491	0.100300	0.000751	100.000
2	13	1.207270	0.000187	0.086777	0.	100.000
2	14	1.244905	0.000219	0.077095	0.	100.000
2	15	1.162710	0.000143	0.100301	0.	100.000
3	1	0.607451	0.000800	0.150213	0.	9.000
3	2	0.933637	0.	0.006626	0.	6.500
3	3	3.844500	0.000627	0.000628	0.	61.200
3	4	0.593056	0.000803	0.150893	0.	43.400
3	5	3.982634	0.000648	0.000677	0.	43.400
3	6	0.793107	0.000444	0.072350	0.	43.500
3	7	0.933149	0.	0.006381	0.	43.600
3	8	0.609331	0.000762	0.142332	0.	100.000
3	9	3.934169	0.000627	0.000626	0.	100.000
3	10	0.780906	0.000727	0.105484	0.	100.000
3	11	0.800677	0.009372	0.099227	0.012583	100.000
3	12	0.802768	0.008413	0.099227	0.011184	100.000
3	13	0.918758	0.000708	0.085826	0.	100.000
3	14	1.005330	0.000699	0.076230	0.	100.000
3	15	0.820122	0.000721	0.099228	0.	100.000

4	1	0.159700	0.019230	0.	15.000
4	2	0.915000	0.000264	0.	13.600
4	3	4.039510	0.012580	0.	150.000
4	4	0.159700	0.019230	0.	100.000
4	5	3.518041	0.012586	0.	125.600
4	6	0.291141	0.010384	0.	125.500
4	7	0.914610	0.000261	0.	124.800
4	8	0.159700	0.019230	0.	150.000
4	9	4.039510	0.012580	0.	150.000
4	10	0.213900	0.017430	0.	150.000
4	11	0.261000	0.102600	0.181400	150.000
4	12	0.258100	0.094250	0.163600	150.000
4	13	0.261000	0.016450	0.	30.000
4	14	0.294200	0.015960	0.	30.000
4	15	0.226900	0.017120	0.	30.000

MESH	COL	MESH	COL	MESH	COL	MESH	COL	MESH	COL	MESH	COL
10.0000	2	5.0000	3	2.5000	4	0.8000	5	0.2972	6	0.1626	7
0.4550	8	1.6839	10	0.4356	11	1.2336	13	0.2048	14	0.2502	15
0.1626	16	0.2972	18	0.1626	19	0.4550	20	2.0902	23	0.4550	24
0.1626	25	0.2972	27	0.1626	28	0.4550	29	0.8999	32	0.4356	33
1.5676	35	0.2048	36	0.2502	37	0.1626	38	0.2972	40	0.1626	41
0.4550	42	2.0902	45	0.4550	46	0.1626	47	0.2972	49	0.1626	50
0.4550	51	2.0902	54	0.4550	55	0.1626	56	0.2972	57	0.6452	59
0.9525	60	2.5000	61	10.0000	62	25.0000	67	50.0000	68		

MESH	ROW	MESH	ROW	MESH	ROW	MESH	ROW	MESH	ROW	MESH	ROW
20.0000	1	10.0000	2	2.5000	3	0.8000	4	0.1016	5	0.1626	6
0.2502	7	2.2267	10	0.2502	11	0.1626	12	0.1016	14	0.1626	15
0.2502	16	1.0020	18	1.3360	20	1.0020	22	0.2502	23	0.1626	24
0.1016	26	0.1626	27	0.2502	28	1.0020	30	1.3360	32	1.0020	34
0.2502	35	0.1626	36	0.1016	38	0.1626	39	0.2502	40	0.2048	41
1.2541	46	0.2048	47	0.2502	48	0.1626	49	0.1016	51	0.1626	52
0.2502	53	1.0020	55	1.3360	57	0.6680	60	0.2502	61	0.1626	62
0.1016	64	0.1626	65	0.2502	66	2.2267	69	0.2502	70	0.1626	71
0.1016	72	0.8000	73	2.5000	74	10.0000	75	20.0000	76		

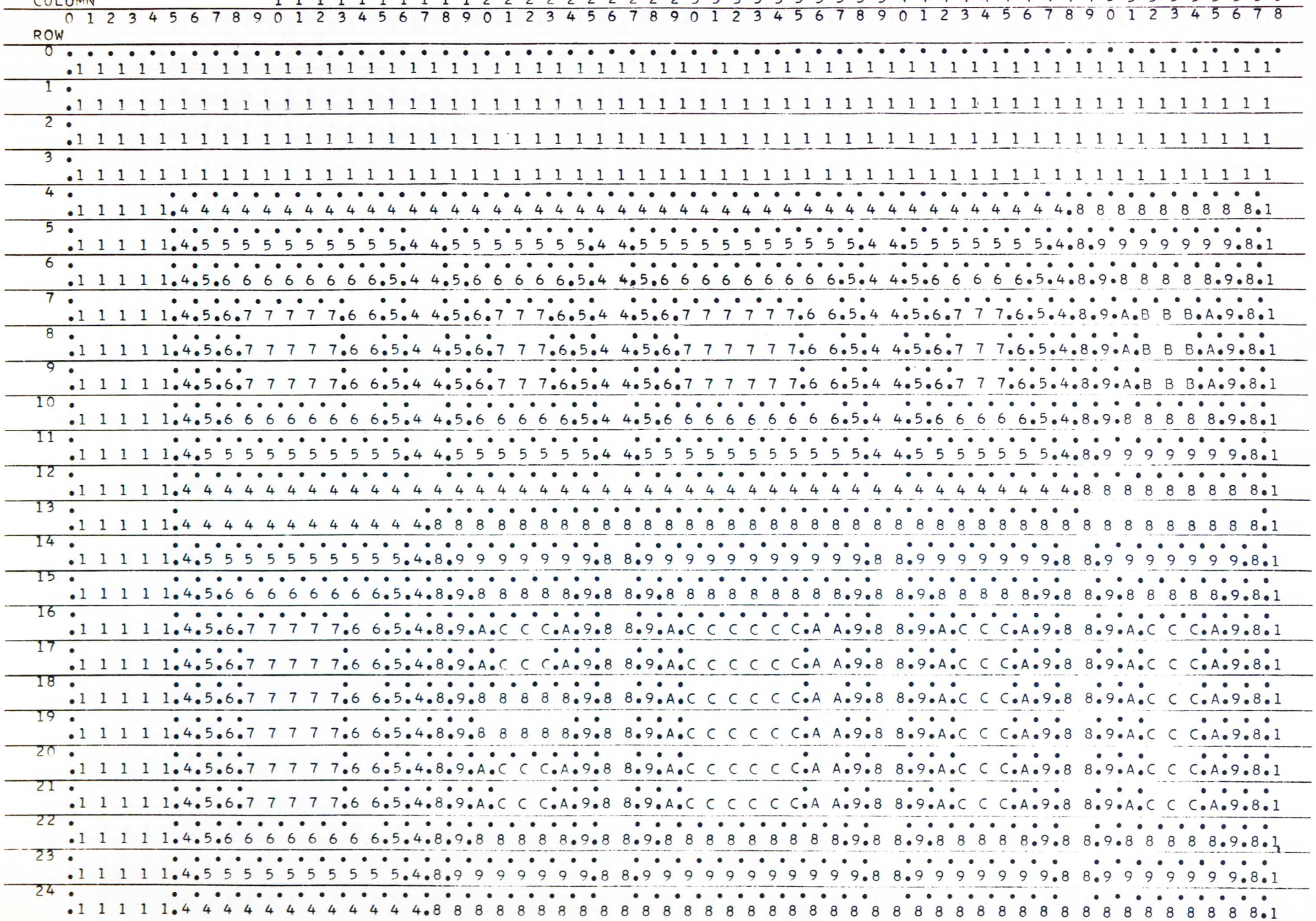
COLUMN
ROW

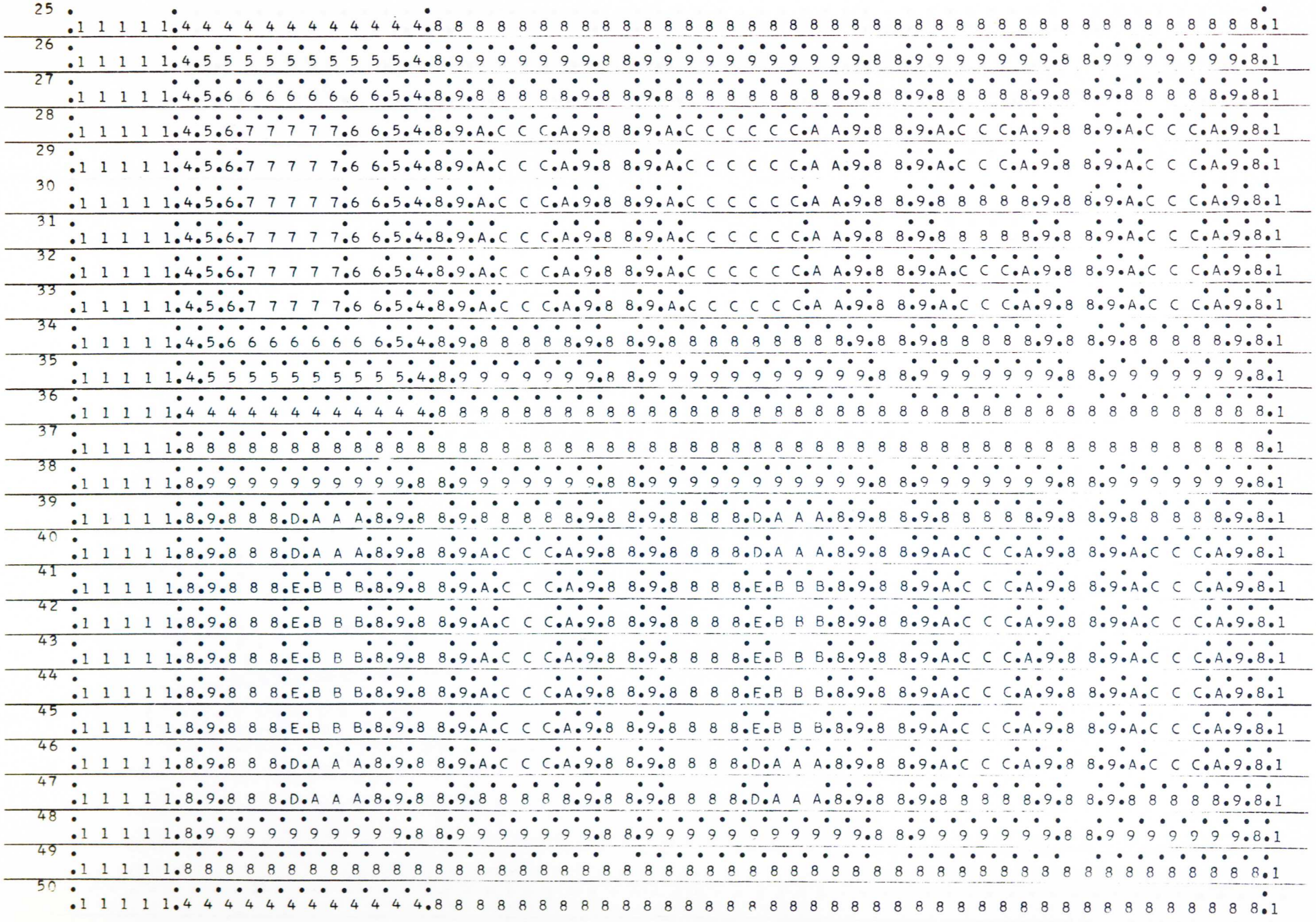

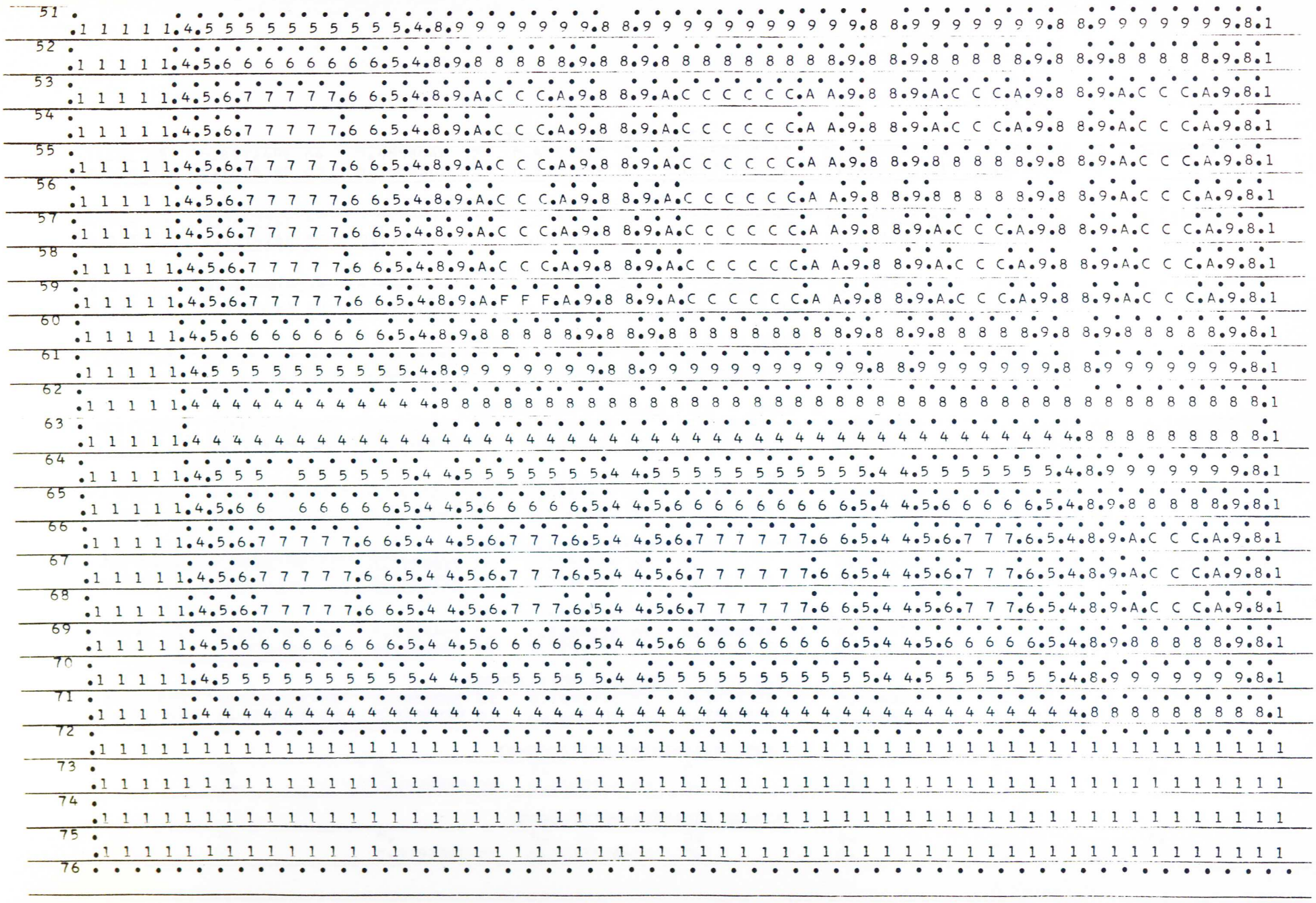

COMPOSITION-INTEGRATED AREA

0.182860E 05	0.897249E 04	0.455804E 02	0.671771E 02	0.525227E 02	0.106388E 03	0.460776E 03	0.288369E 03
0.907209E 02	0.101514E 03	0.795880E 02	0.615764E 03	0.792771E 00	0.546309E 01	0.418890E 01	

COMPOSITION-INTEGRATED FLUX - GROUP 1

0.194754E 03	0.240276E 03	0.263031E 02	0.293460E 02	0.230135E 02	0.461215E 02	0.197020E 03	0.352538E 03
0.115152E 03	0.131426E 03	0.873006E 02	0.882614E 03	0.911907E 00	0.648028E 01	0.312050E 01	

COMPOSITION-AVERAGED FLUX - GROUP 1

0.106504E-01	0.267792E-01	0.577071E 00	0.436845E-00	0.438164E-00	0.433520E-00	0.427583E-00	0.122252E 01
0.126930E 01	0.129466E 01	0.109691E 01	0.143336E 01	0.115028E 01	0.118619E 01	0.744945E 00	

COMPOSITION-INTEGRATED FLUX - GROUP 2

0.242189E 03	0.498493E 03	0.352372E 02	0.360633E 02	0.283247E 02	0.573206E 02	0.251308E 03	0.377734E 03
0.122834E 03	0.139615E 03	0.905875E 02	0.916940E 03	0.979803E 00	0.686595E 01	0.350345E 01	

COMPOSITION-AVERAGED FLUX - GROUP 2

0.132445E-01	0.555579E-01	0.773079E 00	0.536839E 00	0.539285E 00	0.538786E 00	.545401E 00	0.130990E 01
0.135398E 01	0.137533E 01	0.113821E 01	0.148911E 01	0.123592E 01	0.125679E 01	0.836364E 00	

COMPOSITION-INTEGRATED FLUX - GROUP 3

0.290037E 03	0.636135E 03	0.352283E 02	0.368882E 02	0.288569E 02	0.584203E 02	0.252767E 03	0.351966E 03
0.112277E 03	0.126997E 03	0.801264E 02	0.806866E 03	0.913072E 00	0.640766E 01	.326008E 01	

COMPOSITION-AVERAGED FLUX - GROUP 3

0.158611E-01	0.708983E-01	0.772883E 00	0.549119E 00	0.549419E 00	0.549123E 00	0.548568E 00	0.122054E 01
0.123761E 01	0.125104E 01	0.100677E 01	0.131035E 01	0.115175E 01	0.117290E 01	0.778266E 00	

COMPOSITION-INTEGRATED FLUX - GROUP 4

0.213057E 04	0.230729E 04	0.845480E 02	0.123519E 03	0.966062E 02	0.196096E 03	.849333E 03	0.747849E 03
0.213936E 03	0.232681E 03	0.138147E 03	0.125950E 04	0.199293E 01	0.139027E 02	0.717866E 01	

COMPOSITION-AVERAGED FLUX - GROUP 4

0.116513E-00	0.257151E-00	0.185492E 01	0.183871E 01	0.183932E 01	0.184320E 01	0.184327E 01	0.259337E 01
0.235818E 01	0.229211E 01	0.173578E 01	0.204543E 01	0.251387E 01	0.254483E 01	0.171373E 01	

COMPOSITION-INTEGRATED SOURCE

0.	0.	0.	0.	0.	0.	0.	0.
0.	0.	0.262034E 02	0.216296E 03	0.	0.	0.	

COMPOSITION-AVERAGED SOURCE

0.	0.	0.	0.	0.	0.	.	0.
0.	0.	0.329238E-00	0.351264E-00	0.	0.	.	

FIG. 5

CORE CONFIGURATION IN TWO DIMENSIONAL (R,Z) GEOMETRY

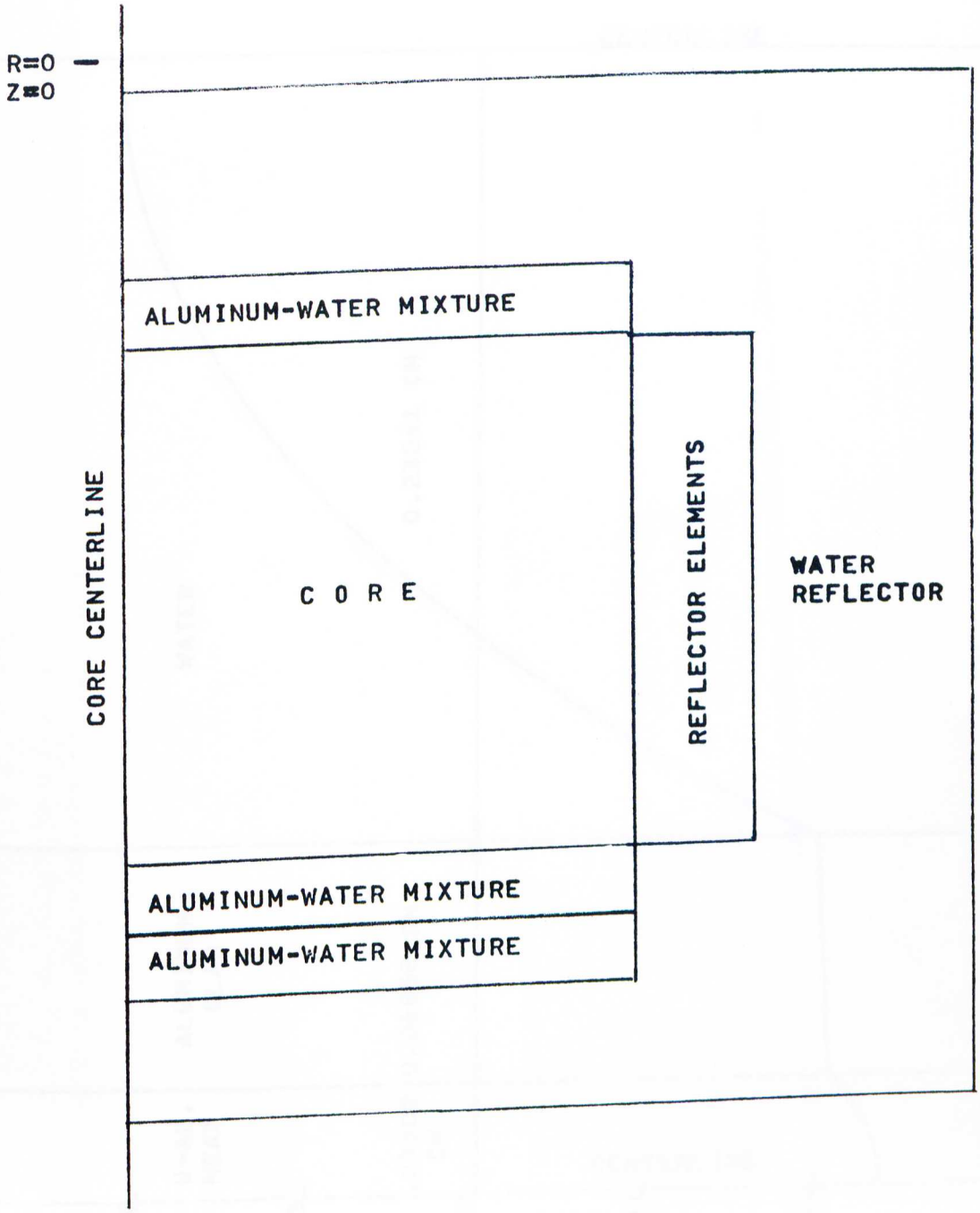

FIG. 6

P-3 APPROXIMATION FOR THERMAL FLUX 16 GRAM PLATE FUEL CELL

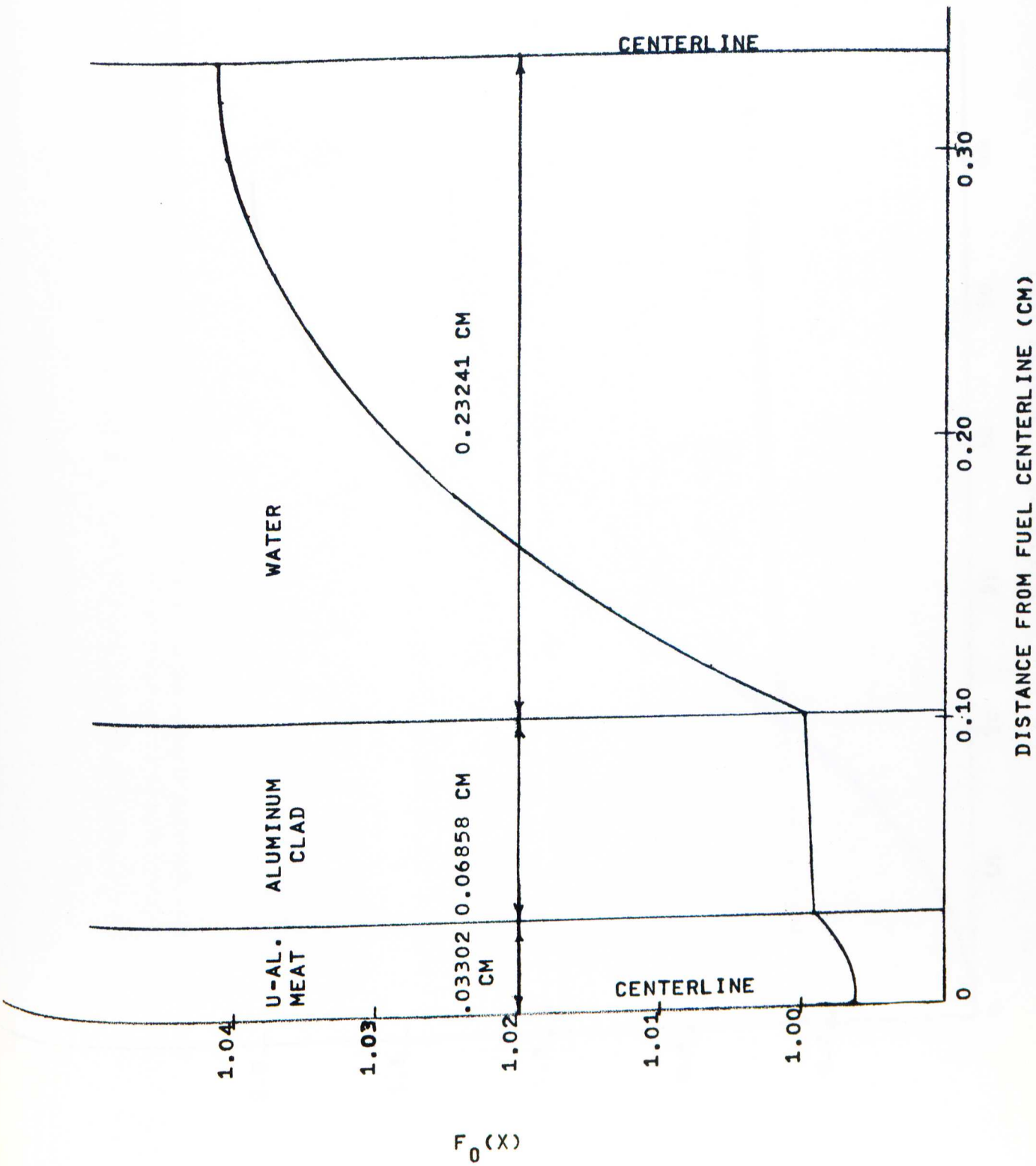

FIG. 7

CONTROL ROD CALIBRATION CURVE FOR SHIM NO. 1

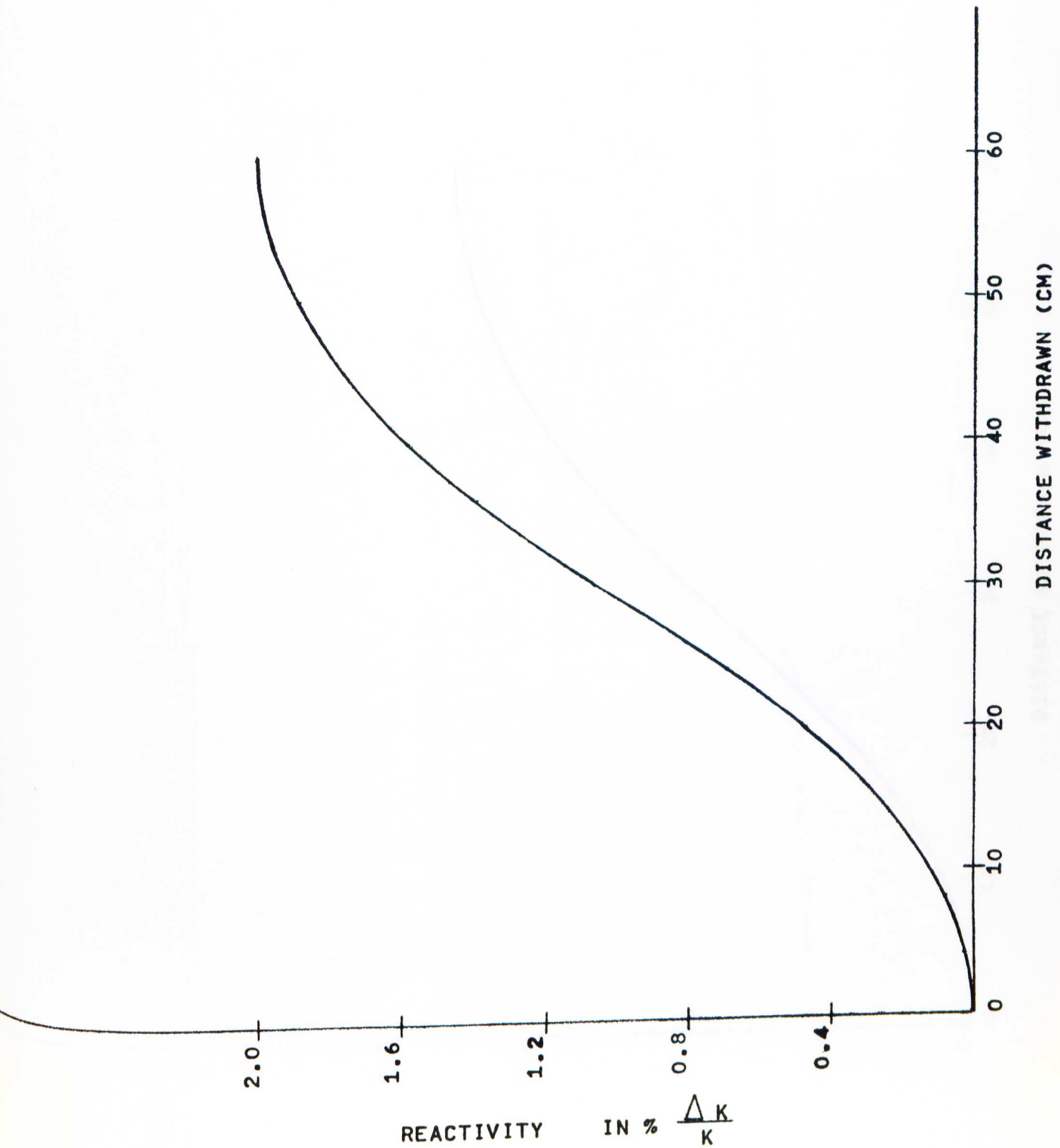

FIG. 8

CONTROL ROD CALIBRATION CURVE FOR SHIM NO. 2

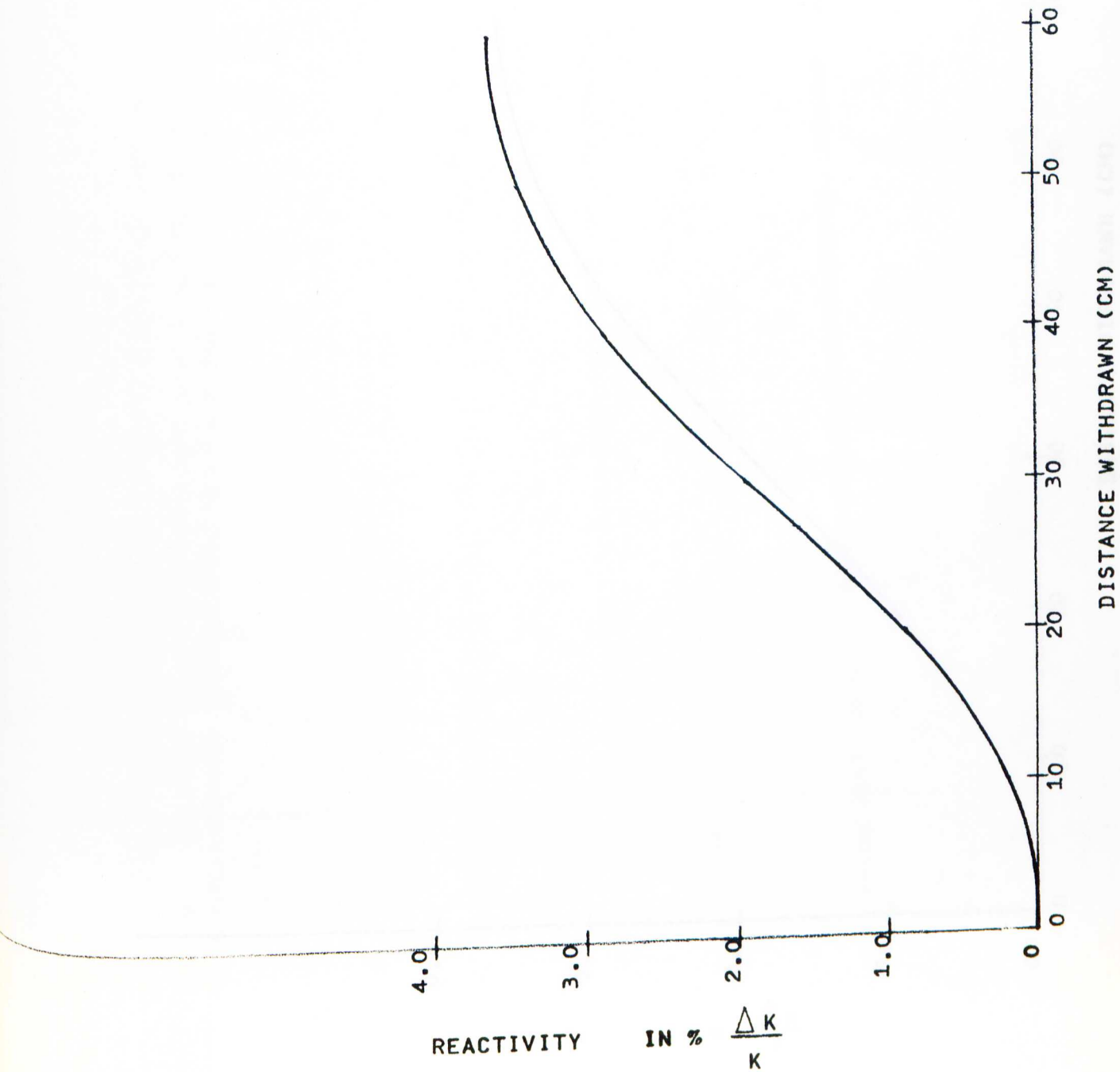

FIG. 9

CONTROL ROD CALIBRATION CURVE FOR REG. ROD

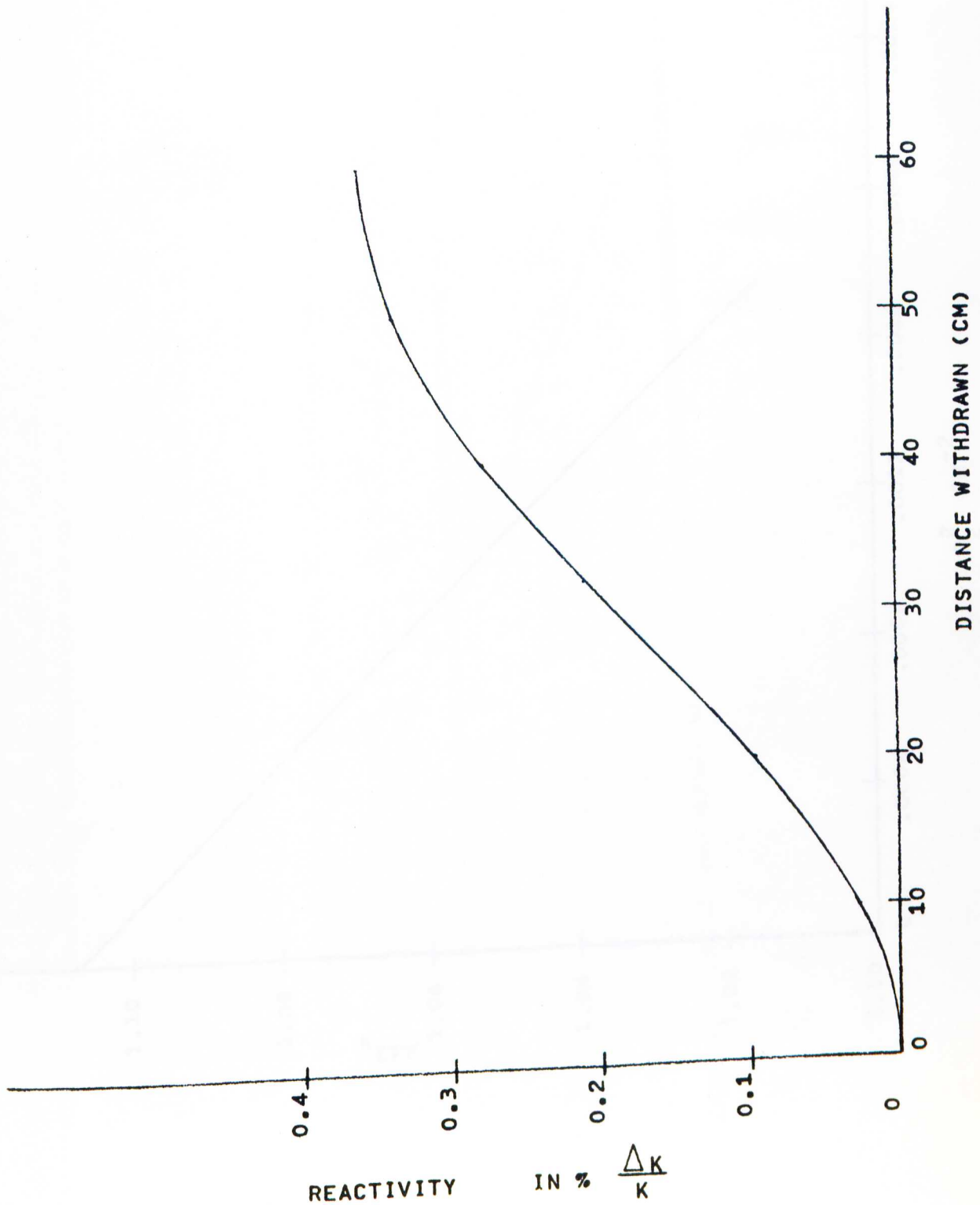

FIG. 10

K_{EFF} VERSUS AXIAL BUCKLING
IN RADIAL WANDA CALCULATIONS

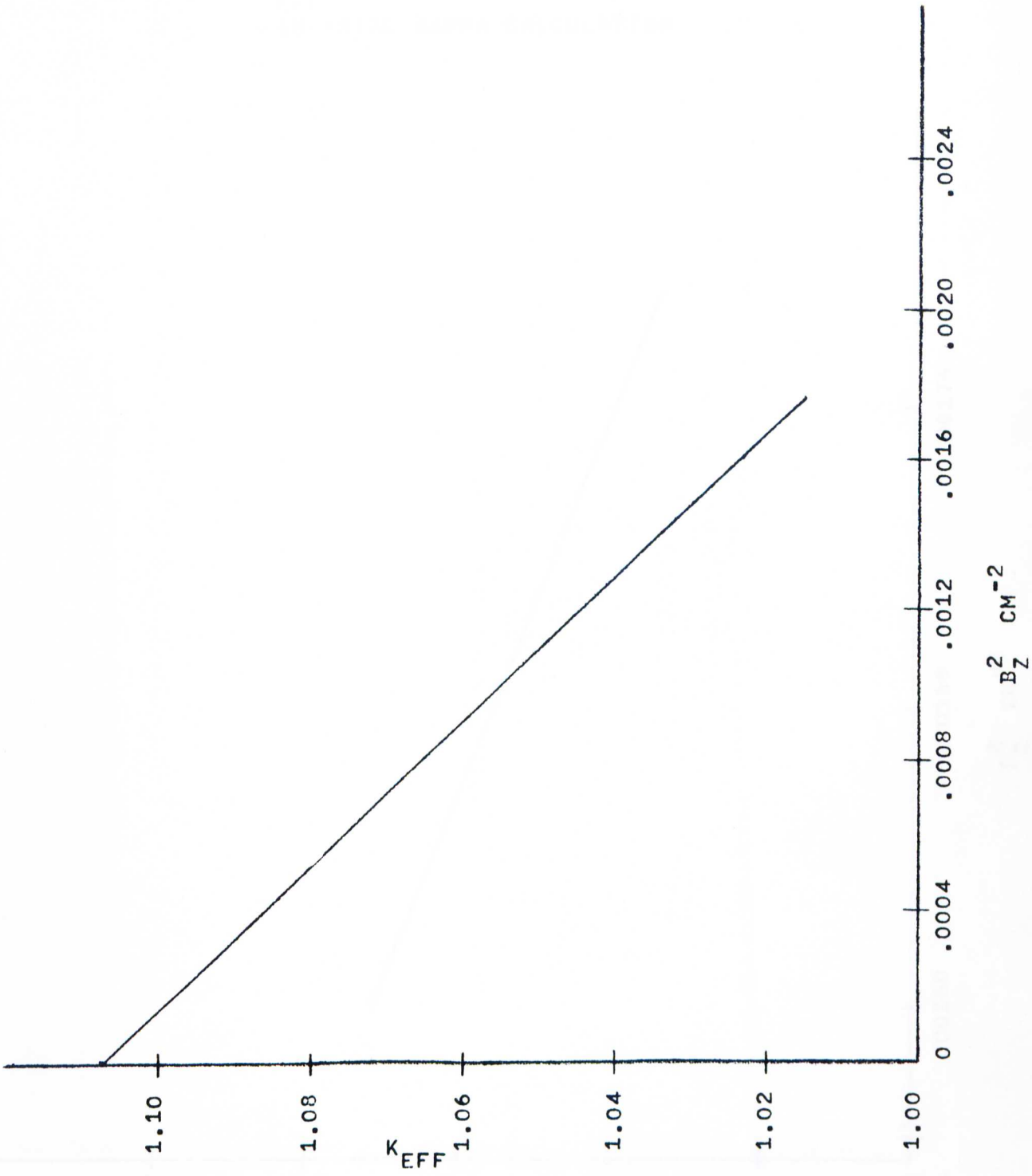

FIG. 11

K_{EFF} VERSUS AXIAL BUCKLING
FOR AXIAL WANDA CALCULATION

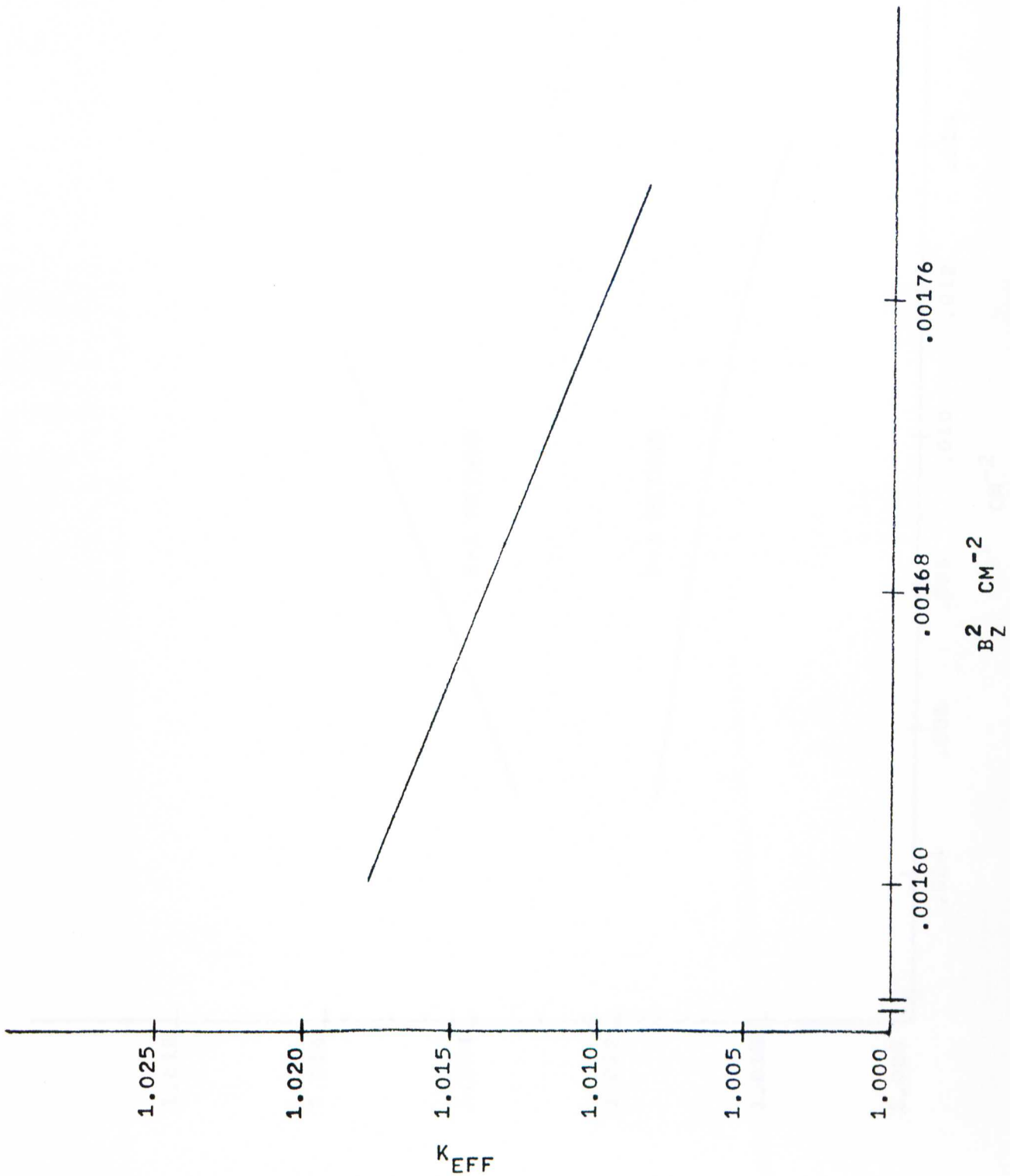

FIG. 12

VARIATION OF CALCULATED CORE K_{EFF} WITH GAM ENERGY INDEPENDENT BUCKLING FOR P-1 AND B-1 METHODS